Li, X., Ge, M., Dai, X., Ren, X., Fritsche, M., Wickert, J., Schuh, H. (2015): Accuracy and reliability of multi-GNSS real-time precise positioning: GPS, GLONASS, BeiDou, and Galileo. - *Journal of Geodesy*, *89*, 6, p. 607-635.

DOI: http://doi.org/10.1007/s00190-015-0802-8

Accuracy and reliability of Multi-GNSS real-time precise positioning: GPS, GLONASS, BeiDou, and Galileo

Xingxing Li[1,2], Maorong Ge[1], Xiaolei Dai[1,2], Xiaodong Ren[2], Mathias Fritsche[1], Jens Wickert[1], and Harald Schuh[1]

1. German Research Centre for Geosciences (GFZ), Telegrafenberg, 14473 Potsdam, Germany; email: lixin@gfz-potsdam.de

2. Wuhan University, 129 Luoyu Road, 430079, Wuhan, Hubei, China;

Abstract: In this contribution, we present a GPS+GLONASS+BeiDou+Galileo four-system model to fully exploit the observations of all these four navigation satellite systems for real-time precise orbit determination, clock estimation and positioning. A rigorous multi-GNSS analysis is performed to achieve the best possible consistency by processing the observations from different GNSS together in one common parameter estimation procedure. Meanwhile, an efficient multi-GNSS real-time precise positioning service system is designed and demonstrated by using the Multi-GNSS Experiment (MGEX), BeiDou Experimental Tracking Network (BETN), and International GNSS Service (IGS) networks including stations all over the world. The statistical analysis of the 6 h predicted orbits show that the radial and cross root mean square (RMS) values are smaller than 10 cm for BeiDou and Galileo, and smaller than 5 cm for both GLONASS and GPS satellites, respectively. The RMS values of the clock differences between real-time and batch-processed solutions for GPS satellites are about 0.10 ns, while the RMS values for BeiDou, Galileo and GLONASS are 0.13, 0.13 and 0.14 ns, respectively. The addition of the BeiDou, Galileo and GLONASS systems to the standard GPS-only processing, reduces the convergence time almost by 70% , while the positioning accuracy is improved by about 25%. Some outliers in the GPS-only solutions vanish when multi-GNSS observations are processed simultaneous. The availability and reliability of GPS precise positioning decrease dramatically as the elevation cutoff increases. However, the accuracy of multi-GNSS precise point positioning (PPP) is hardly decreased and few centimeter are still achievable in the horizontal components even with 40° elevation cutoff. At 30° and 40° elevation cutoffs, the availability rates of GPS-only solution drop significantly to only around 70% and 40% respectively. However, multi-GNSS PPP can provide precise position estimates continuously (availability rate is more than 99.5%) even up to 40° elevation cutoff (e.g., in urban canyons).

Keywords: Multi-GNSS constellation; Real-time Precise Point Positioning; Precise Orbit and Clock Determination; GPS, GLONASS, BeiDou and Galileo

1 Introduction

Besides the already longer time operational Global Navigation Satellite Systems (GNSS) GPS and GLONASS, two additional systems have recently emerged: Galileo and BeiDou. GPS is currently operating at full capability and GLONASS has been revitalized and is also fully operational. Furthermore, both GPS and GLONASS are being modernized (Cai and Gao, 2013). The European Galileo, is the third GNSS, aiming to offer a continuous, more flexible and precise positioning service with a whole set of related parameters and sub-services with importance for broad spectrum of applicants. Four In-Orbit Validation (IOV) satellites have been successfully launched and are in orbit. Currently the IOV phase is closed and it is a transition phase to Full Operational Capability (FOC). The full Galileo constellation will consist of 30 satellites in three orbital planes, including three in-orbit spare ones (Montenbruck et al., 2014). China's BeiDou Navigation Satellite System has been providing continuous positioning, navigation and timing (PNT) services since December 27, 2012, covering the whole Asia-Pacific region. The current BeiDou constellation consists of 5 Geostationary Earth Orbit (GEO), 5 Inclined Geo-Synchronous Orbit (IGSO) and 4 Medium Earth Orbit (MEO) satellites available for PNT services. The next installation phase will complete the constellation, which comprises 5 GEO, 3 IGSO, and 27 MEO satellites by the end of 2020 (China Satellite Navigation Office (CSNO), 2012). Once all four systems are fully deployed, more than 100 satellites will be available for high precision PNT applications.

With the two new and emerging constellations BeiDou and Galileo as well as the ongoing modernization of GPS and GLONASS, the world of satellite navigation is undergoing dramatic changes. The next generation GNSS have the potential to enable a better and wider range of applications for PNT. Already nowadays, much more satellites are in view, transmitting navigation data at more frequencies as during the past years with the dual-frequency system GPS only. The accuracy, reliability and availability of precise positioning will be improved significantly as compared to GPS-only solutions, provided that a combination of the satellite systems is used (Ge et al., 2012, Li et al., 2015). This will also allow for the important shortening of the initialization time in real-time kinematic applications.

In the past the data processing of multi-GNSS was focused on the fusion of GPS and GLONASS (Dach et al., 2006; Cai and Gao, 2013). Thanks to the completion of the constellation of the BeiDou regional system and the establishment of several ground tracking networks, BeiDou precise orbit determination (POD) (Ge et al., 2012; He et al., 2013b; Zhao et al., 2013), GPS/BeiDou combined POD (Shi et al. 2012, Steigenberger et al. 2011; Hauschild et al., 2012; Montenbruck et al., 2012), BeiDou precise point positioning (PPP, Zumberge et al., 1997) (Li et al., 2013a, 2015) and relative positioning (He et al., 2013a; Teunissen et al., 2014) have been investigated recently. Galileo satellite orbits and clocks were determined using ground tracking data from the COoperative Network for GIOVE Observations (CONGO) network as well as the Multi-GNSS Experiment (MGEX) network (e.g. Steigenberger et al., 2011). Initial results on combined GPS/Galileo single-baseline real-time kinematic (RTK) were presented by Odijk and Teunissen (2013).

The International GNSS Service (IGS) has initiated the MGEX since 2012 to enable an early experimentation and familiarization with the emerging new signals and systems as well as to prepare a future, full-featured multi-GNSS service for the scientific community (Montenbruck et al., 2014). Table 1 shows the MGEX analysis centers and related data products (http://www.igs.org/mgex/products). Most of the above mentioned research work and MGEX products are based on single-system or dual-system (e.g., GPS/GLONASS, GPS/Beidou, GPS/Galileo) modes. There is very little research and development on the full exploitation of all the four navigation satellite system, except some commercial advertisement (Chen et al., 2013). Meanwhile, all of the current MGEX products are generated in post-processing mode and only available with a latency of several days or even longer, which cannot satisfy the requirements for time-critical or real-time applications.

Table 1. MGEX Analysis Centers and Products

Institution	ID	Products
CNES/CLS，France	grm	GAL
CODE（AIUB），Switzerland	com	GPS+GLO+GAL
GFZ, Germany	gfm	GPS+GAL, GPS+BDS
ESA/ESOC，Germany	esm	GPS+GAL
JAXA，Japan	qzf	GPS+QZS
TUM，Germany	tum	GAL+QZS
Wuhan Univ.，China	wum	BDS

GFZ, as one of the IGS (International GNSS Service, Dow et al., 2009) real-time data analysis centers, is operationally running its EPOS-RT software (Earth Parameter and Orbit determination System

Real-Time) for providing GPS orbits, clocks, and uncalibrated phase delays (UPDs) for real-time PPP service (Li et al., 2013b, 2013c, 2014). Recently, specific emphasis has been put on adding the GLONASS and the new BeiDou and Galileo satellite systems into the service in order to further improving accuracy, reliability and availability of the real-time services. Extending the GNSS positioning services with additional systems would be beneficial in areas, where the navigation satellite signals are blocked, such as urban areas, or in equatorial zones, where satellite signals may be disturbed or even lost due to ionospheric scintillations (Al-Shaery et al., 2013). It will also help to improve the convergence time of precise positioning.

In this contribution, we present a GPS+GLONASS+BeiDou+Galileo four-system model for real-time PPP as well as POD and precise clock estimation (PCE). A rigorous multi-GNSS analysis is performed to achieve the best possible consistency by processing the observations from different GNSS together in one common parameter estimation procedure. A prototype Multi-GNSS real-time precise positioning service system is designed and realized. Initial results on the achievable orbit and clock quality of four systems, as well as the contribution of multi-GNSS to precise positioning, are presented and analyzed.

This article is organized as follows. We first give an overview of the current status of the four navigation satellite systems and available multi-GNSS tracking data including MGEX, BeiDou Experimental Tracking Network (BETN) and some local Continuously Operating Reference Stations (CORS) networks in Sect. 2. Afterwards, in Sect. 3, the combined BeiDou+Galileo+GLONASS+GPS model and data processing strategy for POD, PCE and PPP are described. We also introduce an efficient procedure for the application in multi-GNSS real-time precise positioning systems and illustrate details. The resulting orbit and clock accuracy as well as real-time positioning performance are evaluated in Sect. 4. A summary of our results and corresponding conclusions are given in Sect. 5.

2 Current Multi-GNSS Status and Available Tracking Network

2.1 Current Status of the Global Navigation Satellite Systems

The U.S. American GPS currently consists of 32 satellites, while for the Russian GLONASS, 24 satellites are in orbit. Both GPS and GLONASS have achieved their full operational capability and are also being gradually modernized. Especially for GLONASS, the FDMA (Frequency Division Multiple Access) mode will be changed to CDMA (Code division multiple access) mode, which is consistent with other GNSSs and convenient for integer ambiguity resolution (Cai and Gao, 2013). Europe's global navigation satellite system Galileo is currently under development. The first pair of satellites was launched on 21 October 2011 and the second pair one year later, on 12 October 2012. These first four IOV satellites have to demonstrate that the space and ground infrastructure of Galileo meet the requirements and they have to validate the system's design in advance of completing the full constellation (http://www.esa.int/Our_Activities/Navigation/The_future_Galileo/What_is_Galileo).

The Chinese BeiDou navigation satellite system is being established independently and pacing steadily forward towards an operational global navigation satellite system by 2020. The two-phase schedule enables its rapid emerging to a global system starting with operational services over the Asia-Pacific region first. The initial BeiDou phase consists of five satellites in GEO at an altitude of 35,786 km, five in IGSO at an altitude of 35, 786 km as well as with 55° inclination to the equatorial plane, and four in MEO at an altitude of 21, 528 km and 55° inclination to the equatorial plane (Yang et al., 2011; CSNO 2012). The details of the satellites currently in orbit are listed in Table 2.

Table 2. Satellites of the current BeiDou constellation (as of end 2014).

Satellite	PRN	NORAD-ID	COSPAR-ID	Launch Date	Mean Longitude (inclination)
G1	C01	36287	2010-001A	16/01/2010	140.0°E
G2	C02	34779	2009-017A	14/04/2009	Drift
G3	C02	36590	2010-024A	02/06/2010	80.0°E
G4	C04	37210	2010-057A	31/10/2010	160.0°E
G5	C05	38091	2012-008A	14/02/2012	58.7°E
G6	C03	38953	2012-059A	25/10/2012	110.5°E
I1	C06	36828	2010-036A	31/07/2010	122.0°E (55.0°)
I2	C07	37256	2010-068A	17/12/2010	119.0°E (55.0°)
I3	C08	37384	2011-013A	09/04/2011	120.0°E (55.0°)
I4	C09	37763	2011-038A	26/07/2011	96.5°E (55.0°)
I5	C10	37948	2011-073A	01/12/2011	92.5°E (55.0°)
M1	C30	31115	2007-011A	13/04/2007	Discarded
M3	C11	38250	2012-018A	29/04/2012	(55.0°)
M4	C12	38251	2012-018B	29/04/2012	(55.0°)
M5	C13	38774	2012-050A	18/09/2012	(55.0°)
M6	C14	38775	2012-050B	18/09/2012	(55.0°)

Table 3 summarizes the current GNSS status including satellite type, transmitted signals, and available satellite number (Montenbruck et al., 2014).

Table 3. Deployment status of current multi-GNSS (* denotes non-operational satellite)

System	Blocks	Signals	Sats
GPS	IIA	L1 C/A,L1/L2 P(Y)	6
	IIR-A/B	L1C/A,L1/L2	12
	IIR-M	+L2C	7
	IIF	+L5	7
GLONASS	M	L1/L2 C/A+P	24
	K	+L3	1*
BeiDou	GEO	B1,B2,B3	5
	IGSO	B1,B2,B3	5
	MEO	B1,B2,B3	4

Galileo	IOV	E1,(E6), E5a/b/ab	4*

Figure 1 shows a 24 h ground track of the four systems satellites available for positioning on September 1, 2013. As Figure 1 shows, the ground tracks of the five BeiDou IGSOs are confined from approximately 55°S to 55°N latitude and 102°E to 135°E longitude. The IGSO satellites describe figure-of-eight loops, while the GEO satellites are fixed in longitude but with small variation in the latitude by up to 2°. Five GEOs are distributed in the Indian and Pacific oceans over the Equator as supplements for the IGSO satellites to ensure users in Asian-Pacific regions can observe enough satellites. They are located at the 58.75°E, 80.0°E, 110.5°E, 140.0°E, and 160°E longitudes, respectively.

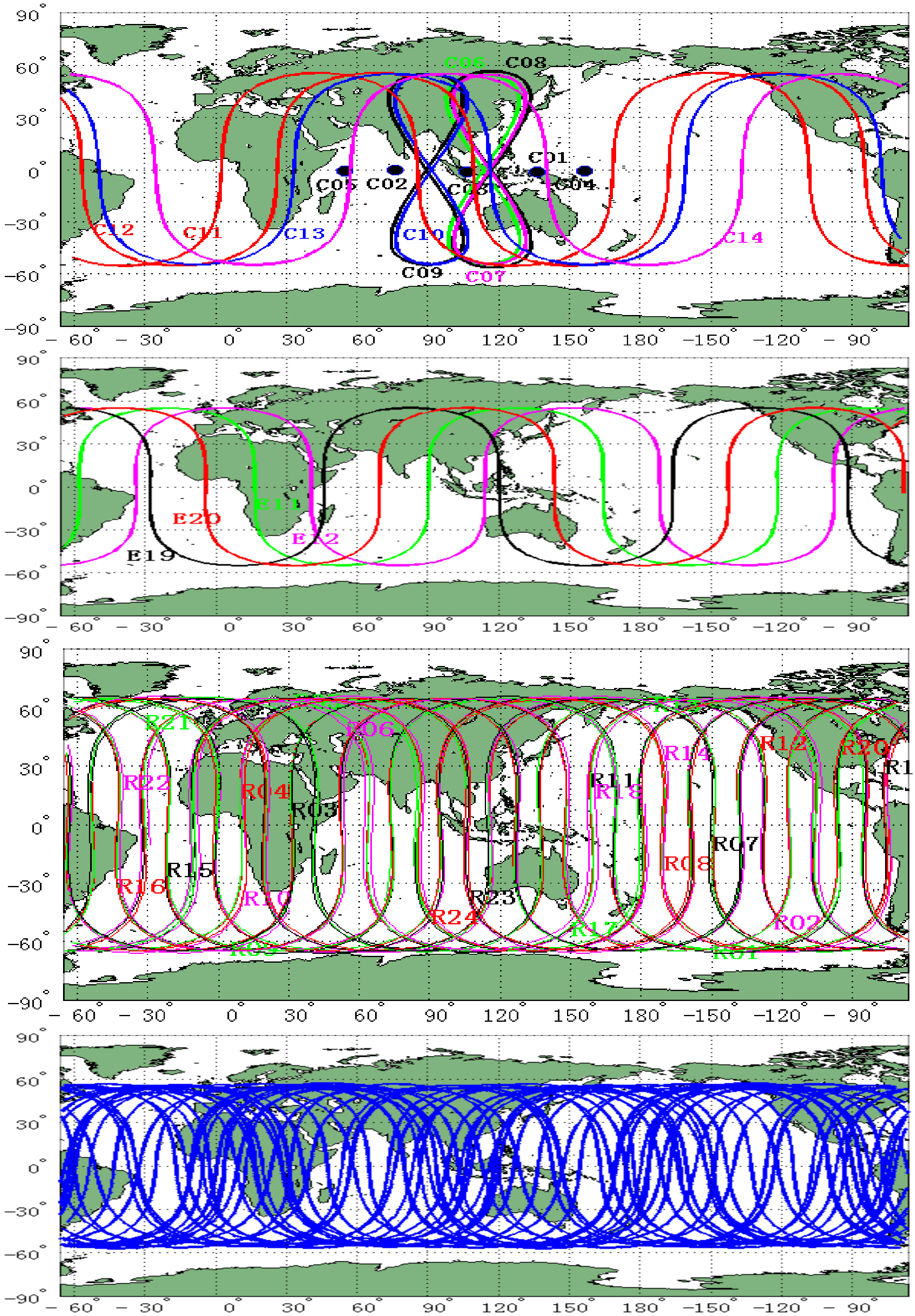

Figure 1. Ground tracks of four satellite navigation systems as of September 2013: BeiDou, Galileo,

GLONASS and GPS, from top to down; The different colors and times are selected only for better distinction and display of trajectories.

2.2 Available GNSS Ground Tracking Networks

The MGEX is an initiative from the IGS to collect and analyze data from GPS, GLONASS, BeiDou and Galileo. As a backbone of the MGEX project, a new network of multi-GNSS monitoring stations has been deployed around the globe in parallel to the legacy IGS network for GPS and GLONASS tracking. Building on volunteer contributions from various national agencies, universities, and other institutions, the MGEX network was consisting of almost 90 stations by September 2013 (Montenbruck et al., 2014). As a minimum, all MGEX stations support the tracking of GPS as well as one of the new BeiDou, Galileo, or QZSS constellations. While not a prerequisite, GLONASS is likewise supported by the majority of stations. About 75 stations are tracking the Galileo satellites, whereas BeiDou is tracked by 25 receivers, see Figure 2.

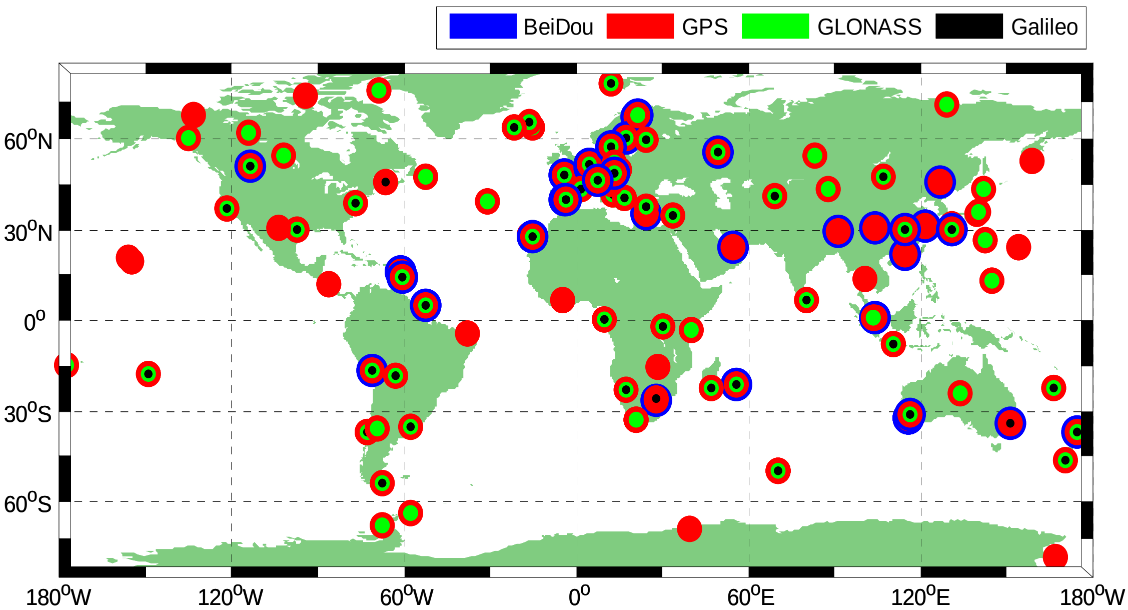

Figure 2. Distribution of MGEX stations and their supported constellations (as of September 2013); some IGS stations (the red circles, GPS-only) are also included.

In order to assess the precise positioning performance of the BeiDou system, Wuhan University has established a continuous worldwide observation reference network since 2011, called the BETN, which includes nine tracking stations in China and six tracking stations abroad (Shi et al., 2012). The stations in China are BJF1 in Beijing, CENT in Wuhan, CHDU in Chengdu, HRBN in Harbin, HKTU at Hong Kong, NTSC and XIAN at Xi'an city, SHAO in Shanghai, and LASA in Tibet. The five oversea stations are SIGP (Singapore), PETH (Australia), DHAB (the United Arab Emirates), LEID (Netherlands), and JOHA (South Africa). Figure 3 shows the global distribution of the BETN. All the stations are equipped with the UB240-CORS dual-frequency and GPS/BeiDou dual-system receivers and the UA240 antennas manufactured by the UNICORE Company in China (He et al., 2013b). The Unicore UA240 dual-frequency (B1, B2) dual-system high gain antenna is used in the network.

Besides the above mentioned networks, a local HuBei CORS network with six stations equipped with the same UNICORE receiver and antenna are also employed as user stations for test of precise positioning performance. The inter-station distance is about several tens of km on average and is deployed for Network Real-Time Kinematic (NRTK) positioning with GPS and planned to be extended for GPS and BeiDou multi-GNSS service. The distribution of the stations and the location referred to the BETN network are shown on Figure 3.

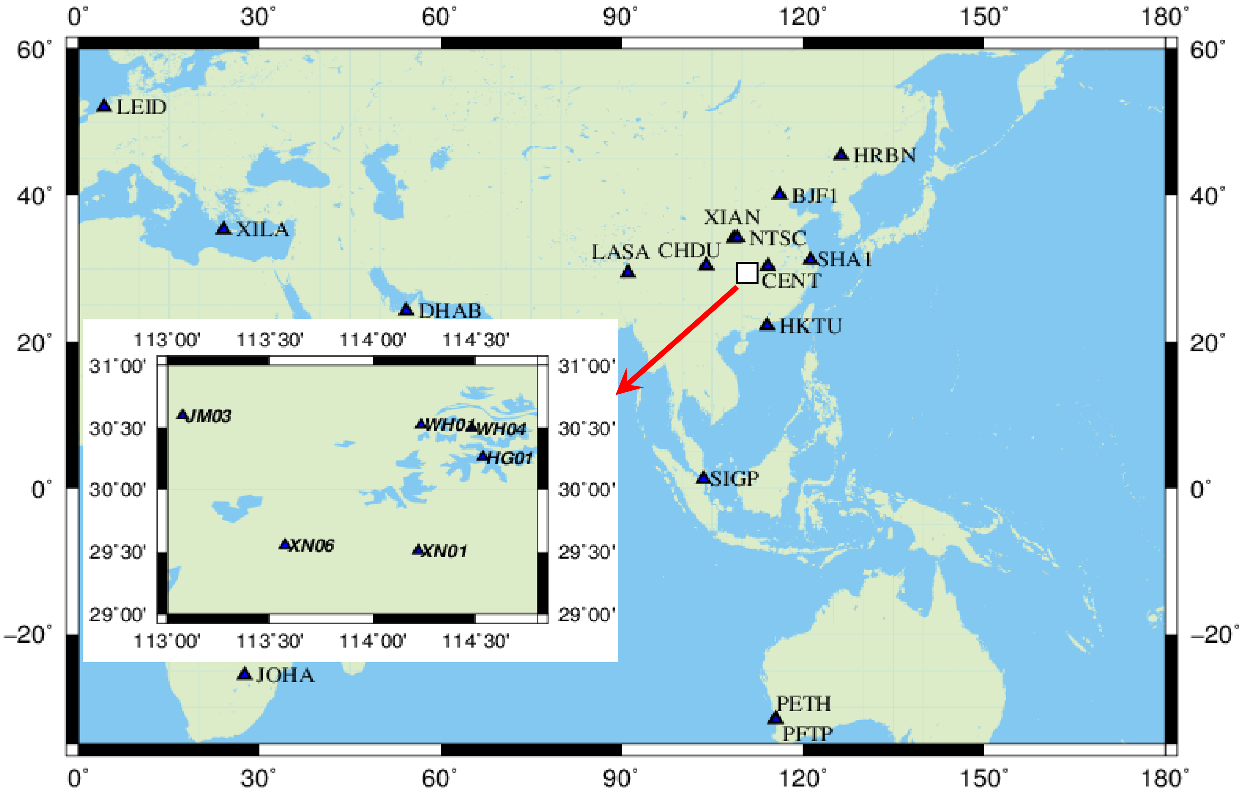

Figure 3. BETN and a local CORS network equipped with GPS+BeiDou capable dual-system receivers. The small map indicates the local CORS network and the large one is for BETN.

3 Multi-GNSS Real-time Precise Positioning

3.1 General multi-GNSS observation model

The observation equations for undifferenced (UD) carrier phase L and pseudorange P respectively, can be expressed as following:

$$L_{r,j}^{s} = \rho_{r\,g}^{s} - t^{s} + t_{r} + \lambda_{j}(b_{r,j} - b_{j}^{s}) + \lambda_{j} N_{r,j}^{s} - I_{r,j}^{s} + T_{r}^{s} + \varepsilon_{r,j}^{s} \quad (1)$$

$$P_{r,j}^{s} = \rho_{r\,g}^{s} - t^{s} + t_{r} + c(d_{r,j} - d_{j}^{s}) + I_{r,j}^{s} + T_{r}^{s} + e_{r,j}^{s} \quad (2)$$

where indices s, r, and j refer to the satellite, receiver, and carrier frequency, respectively; t^{s} and t_{r} are the clock biases of satellite and receiver; $N_{r,j}^{s}$ is the integer ambiguity; $b_{r,j}$ and b_{j}^{s} are the receiver- and satellite-dependent uncalibrated phase delay (Ge et al., 2008; Li et al., 2011); λ_{j} is the wavelength;

$d_{r,j}$ and $d_j^{\,s}$ are the code biases of the receiver and the satellite; $I_{r,j}^s$ is the ionospheric delay of the signal path at frequency j; T_r^s is the frequency independent tropospheric delay; $e_{r,j}^s$ and $\varepsilon_{r,j}^s$ denote the sum of measurement noise and multipath error for the pseudorange and carrier phase observations. Furthermore, ρ_g denotes the geometric distance between the phase centers of the satellite and receiver antennas at the signal transmitting and receiving time, respectively. This means, that the phase center offsets and variations and earth tides must be considered. Phase wind-up and relativistic delays must also be corrected according to the existing models (Kouba, 2009), although they are not included in the equations.

The slant tropospheric delay consists of the dry and wet components and both can be expressed by their individual zenith delay and mapping function. The tropospheric delay is usually corrected for its dry component with an a priori model, while the residual part of the tropospheric delay (considered as zenith wet delay Z_r) at the station r is estimated from the observations.

$$L_{r,j}^s = \rho_{r\,gT}^s - t^s + t_r + \lambda_j (b_{r,j} - b_j^{\,s}) + \lambda_j N_{r,j}^s - I_{r,j}^s + m_r^s \cdot Z_r + \varepsilon_{r,j}^s \tag{3}$$

$$P_{r,j}^s = \rho_{r\,gT}^s - t^s + t_r + c(d_{r,j} - d_j^{\,s}) + I_{r,j}^s + m_r^s \cdot Z_r + e_{r,j}^s \tag{4}$$

where m_r^s is the wet mapping function, $\rho_{r\,gT}^s$ is the geometric distance plus dry tropospheric delay.

For multi-frequency observations, the ionospheric delays at different frequencies can be expressed as,

$$I_{r,j}^s = \kappa_j \cdot I_{r,1}^s, \; where\; \kappa_j = \lambda_j^{\,2} / \lambda_1^{\,2} \tag{5}$$

The first order of ionospheric delays can be eliminated by forming a linear combination of observations at different frequencies. Usually, the ionosphere-free observation is used for the network solution (e.g. POD, PCE) and PPP (Kouba and Héroux, 2001). Alternatively, the dual-frequency data can be separately processed where the slant ionospheric delays are estimated in the raw observations (Schaffrin and Bock, 1988; Li et al., 2013b). In order to strengthen the solution, a priori knowledge of the ionospheric delays including the temporal correlation, and spatial characteristics and external ionospheric model can be utilized to constrain the estimated ionospheric parameters (Li et al., 2013b). These constraints, to be imposed on observations of a single station can be summarized as:

$$\begin{aligned} & I^s_{r,t} - I^s_{r,t-1} = w_t, w_t \sim N(0, \sigma^2_{wt}) \\ & vI^s_r = I^s_r / f^s_{r,IPP} = a_0 + a_1 dL + a_2 dL^2 + a_3 dB + a_4 dB^2, \sigma^2_{vI} \\ & I^s_r = \tilde{I}^s_r, \sigma^2_{\tilde{I}} \end{aligned} \tag{6}$$

where t is the current epoch and $t-1$ is the previous epoch; w_t is a zero mean white noise with variance σ^2_{wt}; vI^s_r is the vertical ionospheric delay with a variance of σ^2_{vI}; $f^s_{r,IPP}$ is the mapping function at the ionospheric pierce point (IPP); the coefficients a_i describe the trend; dL and dB are the longitude and latitude difference between the IPP and the station location; $\tilde{I}^s_r$ is the ionospheric delay obtained from external ionospheric model with a variance of $\sigma^2_{\tilde{I}}$. In the network solution case, a spatial ionospheric model can also be employed to represent the spatial correlation of ionospheric delay parameters at different stations (Schaffrin and Bock, 1988).

For formulation, the ionosphere-free model is a simplification of the raw-observation model. Therefore, we will hereafter focus on raw-observation model for equation expression. The linearized equations for (3) and (4) can be expressed as follows,

$$l^s_{r,j} = \mathbf{u}^s_r \cdot \psi(t,t_0)^s \cdot \mathbf{o}_0{}^s - \mathbf{u}^s_r \cdot \mathbf{r}_r - t^s + t_r + \lambda_j (b_{r,j} - b_j{}^s) + \lambda_j N^s_{r,j} - \kappa_j \cdot I^s_{r,1} + m^s_r \cdot Z_r + \varepsilon^s_{r,j} \tag{7}$$

$$p^s_{r,j} = \mathbf{u}^s_r \cdot \psi(t,t_0)^s \cdot \mathbf{o}_0{}^s - \mathbf{u}^s_r \cdot \mathbf{r}_r - t^s + t_r + c(d_{r,j} - d_j{}^s) + \kappa_j \cdot I^s_{r,1} + m^s_r \cdot Z_r + e^s_{r,j} \tag{8}$$

$$\mathbf{o}_0{}^s = (x_0{}^s \ y_0{}^s \ z_0{}^s \ \dot{x}_0{}^s \ \dot{y}_0{}^s \ \dot{z}_0{}^s \ p^s_1 \ p^s_2 \cdots p^s_n)^T \tag{9}$$

where $l^s_{r,j}$ and $p^s_{r,j}$ denote "observed minus computed" phase and pseudorange observables from satellite s to receiver r at the frequency j; $\mathbf{u}^s_r$ is the unit vector of the direction from receiver to satellite; $\mathbf{r}_r$ denotes the vector of the receiver position increments relative to a priori position which is used for linearization; $\mathbf{o}_0{}^s$ denotes initial orbit state for satellite s; $\psi(t,t_0)$ denotes state transition matrix from initial epoch t_0 to current epoch t; $x_0{}^s$, $y_0{}^s$ and $z_0{}^s$ are the initial position; $\dot{x}_0{}^s$, $\dot{y}_0{}^s$ and $\dot{z}_0{}^s$ are the initial velocity; $p_1^s, p_2^s, \cdots p_n^s$ are solar radiation pressure parameters.

In multi-constellation case, the combined GPS+GLONASS+Galileo+BeiDou observation model can be expressed as,

$$
\begin{aligned}
l_{r,j}^{G} &= \mathbf{u}_r^G \cdot \psi(t,t_0)^G \cdot \mathbf{o}_0{}^G - \mathbf{u}_r^G \cdot \mathbf{r}_r - t^G + t_r + \lambda_{jG}(b_{rG,j} - b_j{}^G) + \lambda_{jG} N_{r,j}^G - \kappa_{jG} \cdot I_{r,1}^G + m_r \cdot Z_r + \varepsilon_{r,j}^G \\
l_{r,j}^{R_k} &= \mathbf{u}_r^R \cdot \psi(t,t_0)^R \cdot \mathbf{o}_0{}^R - \mathbf{u}_r^R \cdot \mathbf{r}_r - t^R + t_r + \lambda_{jR_k}(b_{rR_k,j} - b_j{}^R) + \lambda_{jR_k} N_{r,j}^R - \kappa_{jR_k} \cdot I_{r,1}^R + m_r \cdot Z_r + \varepsilon_{r,j}^R \\
l_{r,j}^{E} &= \mathbf{u}_r^E \cdot \psi(t,t_0)^E \cdot \mathbf{o}_0{}^E - \mathbf{u}_r^E \cdot \mathbf{r}_r - t^E + t_r + \lambda_{jE}(b_{rE,j} - b_j{}^E) + \lambda_{jE} N_{r,j}^E - \kappa_{jE} \cdot I_{r,1}^E + m_r \cdot Z_r + \varepsilon_{r,j}^E \\
l_{r,j}^{C} &= \mathbf{u}_r^C \cdot \psi(t,t_0)^C \cdot \mathbf{o}_0{}^C - \mathbf{u}_r^C \cdot \mathbf{r}_r - t^C + t_r + \lambda_{jC}(b_{rC,j} - b_j{}^C) + \lambda_{jC} N_{r,j}^C - \kappa_{jC} \cdot I_{r,1}^C + m_r \cdot Z_r + \varepsilon_{r,j}^C
\end{aligned}
\tag{10}
$$

$$
\begin{aligned}
p_{r,j}^{G} &= \mathbf{u}_r^G \cdot \psi(t,t_0)^G \cdot \mathbf{o}_0{}^G - \mathbf{u}_r^G \cdot \mathbf{r}_r - t^G + t_r + c(d_{rG,j} - d_j{}^G) + \kappa_{jG} \cdot I_{r,1}^G + m_r \cdot Z_r + e_{r,j}^G \\
p_{r,j}^{R_k} &= \mathbf{u}_r^R \cdot \psi(t,t_0)^R \cdot \mathbf{o}_0{}^R - \mathbf{u}_r^R \cdot \mathbf{r}_r - t^R + t_r + c(d_{rR_k,j} - d_j{}^R) + \kappa_{jR_k} \cdot I_{r,1}^R + m_r \cdot Z_r + e_{r,j}^R \\
p_{r,j}^{E} &= \mathbf{u}_r^E \cdot \psi(t,t_0)^E \cdot \mathbf{o}_0{}^E - \mathbf{u}_r^E \cdot \mathbf{r}_r - t^E + t_r + c(d_{rE,j} - d_j{}^E) + \kappa_{jE} \cdot I_{r,1}^E + m_r \cdot Z_r + e_{r,j}^E \\
p_{r,j}^{C} &= \mathbf{u}_r^C \cdot \psi(t,t_0)^C \cdot \mathbf{o}_0{}^C - \mathbf{u}_r^C \cdot \mathbf{r}_r - t^C + t_r + c(d_{rC,j} - d_j{}^C) + \kappa_{jC} \cdot I_{r,1}^C + m_r \cdot Z_r + e_{r,j}^C
\end{aligned}
\tag{11}
$$

where indices G, R, E and C refer to the GPS, GLONASS, Galileo, and BeiDou satellite systems, respectively; R_k denotes the GLONASS satellite with frequency factor k that are used for the computation of the carrier phase frequencies of the individual GLONASS satellites; d_{rG}, d_{rR_k}, d_{rE}, and d_{rC} denote the code biases of the receiver r for G, R, E and C, respectively.

3.2 The inter-system/inter-frequency biases

Because of the different frequencies and signal structure of the individual GNSS, the code bias values d_{rG}, d_{rR_k}, d_{rE}, and d_{rC} are different in one multi-GNSS receiver. The differences between them are usually called inter-system biases (ISB) for code observations. Similarly, the phase delays b_{rG}, b_{rR_k}, b_{rE} and b_{rC} are also different and their differences are inter-system biases for phase observations. As

GLONASS satellites emit the signals on individual frequencies, it will also lead to frequency-dependent biases in the receivers. For the GLONASS satellites with different frequency factors, the receiver code bias d_{rR_k}, as well as phase delay b_{rR_k}, are different. Their differences are usually called inter-frequency biases (IFB).

Of course, the inter-system and inter-frequency biases must be considered in a combined analysis of multi-GNSS data. Consequently, corresponding parameters have to be estimated for all multi-GNSS receivers: one bias for the code measurements of each system (each frequency for GLONASS) was setup for each station. Because the receiver and satellite clocks are also computed, two singularities have to be treated. The code bias for GPS satellites of each station is set to zero. Here the ionosphere-free linear combination from P1 and P2 is defined as reference and the differential code biases (DCBs) are introduced to consider different code types. This means that all computed biases of other systems are obtained relative to the biases for the GPS observations. These estimated biases can be interpreted as a relative calibration of “BeiDou/Galileo with respect to GPS” and “each individual frequency used by a GLONASS satellite with respect to the GPS frequency”. Meanwhile, we introduce zero mean conditions over all estimated ISB and IFB: the sum of the biases of all stations for each system (i.e. BeiDou and Galileo) and each GLONASS frequency is set to zero. These zero mean conditions are equivalent to fixing all code biases of one receiver to any value. For n stations and k GLONASS frequency factors, the zero mean conditions can be expressed as,

$$\begin{aligned}
&d_{1C}+d_{2C}+d_{3C}+\cdots+d_{nC}=0\\
&d_{1E}+d_{2E}+d_{3E}+\cdots+d_{nE}=0\\
&d_{1R_1}+d_{2R_1}+d_{3R_1}+\cdots+d_{nR_1}=0\\
&d_{1R_2}+d_{2R_2}+d_{3R_2}+\cdots+d_{nR_2}=0\\
&d_{1R_3}+d_{2R_3}+d_{3R_3}+\cdots+d_{nR_3}=0\\
&\qquad\qquad\vdots\\
&d_{1R_k}+d_{2R_k}+d_{3R_k}+\cdots+d_{nR_k}=0
\end{aligned} \tag{12}$$

The inter-system/inter-frequency biases and the obtained satellite clocks are fully correlated. This means that, when using the satellite clocks, e.g., for a PPP of further stations, corresponding biases have also to be estimated or corrected for these GNSS receivers. It is worthwhile to notice that such a receiver internal bias is relevant only if processing the code data. When analyzing the phase measurements the corresponding phase ambiguity parameters will absorb the phase delays. They become only relevant if ambiguities are resolved to their integer values, i.e. mixed ambiguity resolution between different GNSS, GLONASS ambiguity resolution or undifferenced ambiguity resolution.

To obtain consistent products for different GNSS, a rigorous combined analysis of measurements from all systems is preferable. We perform a rigorous GNSS analysis by processing all the observations from different GNSS together in one common parameter adjustment procedure. On one hand, the resulting orbits and clock corrections for different GNSS have the fully consistency. On the other hand, this strategy requires a higher computer performance because of the higher number of observations that have to be processed together and because of the higher number of parameters that have to be solved for. For each frequency factor (usually one pair of satellites) one additional parameter has to be solved for when the receiver and satellite clocks are computed. The estimation of inter-system and inter-frequency biases for each GNSS station introduces a big number of additional parameters, especially when computing GLONASS satellite clock corrections. In consideration of computation efficiency, biases that are computed from a certain time interval for a station can later be applied for the analysis as it is done today with the differential code biases (Schaer et al., 1999; Dach et al., 2006).

3.3 Application to POD, PCE and PPP

For a real-time precise positioning service, at least three components including POD, PCE and PPP are necessary, while another two, namely UPD estimation and ionospheric modeling are optional and help to improve the positioning performance. In POD procedure, the station positions are fixed (or tightly constrained) to well-known values,

$$\begin{aligned}
l_{r,j}^{G} &= \mathbf{u}_r^G \cdot \psi(t,t_0)^G \cdot \mathbf{o}_0{}^G - t^G + t_r + \lambda_{jG}(b_{rG,j} - b_j{}^G) + \lambda_{jG} N_{r,j}^G - \kappa_{jG} \cdot I_{r,1}^G + m_r \cdot Z_r + \varepsilon_{r,j}^G \\
l_{r,j}^{R_k} &= \mathbf{u}_r^R \cdot \psi(t,t_0)^R \cdot \mathbf{o}_0{}^R - t^R + t_r + \lambda_{jR_k}(b_{rR_k,j} - b_j{}^R) + \lambda_{jR_k} N_{r,j}^R - \kappa_{jR_k} \cdot I_{r,1}^R + m_r \cdot Z_r + \varepsilon_{r,j}^R \\
l_{r,j}^{E} &= \mathbf{u}_r^E \cdot \psi(t,t_0)^E \cdot \mathbf{o}_0{}^E - t^E + t_r + \lambda_{jE}(b_{rE,j} - b_j{}^E) + \lambda_{jE} N_{r,j}^E - \kappa_{jE} \cdot I_{r,1}^E + m_r \cdot Z_r + \varepsilon_{r,j}^E \\
l_{r,j}^{C} &= \mathbf{u}_r^C \cdot \psi(t,t_0)^C \cdot \mathbf{o}_0{}^C - t^C + t_r + \lambda_{jC}(b_{rC,j} - b_j{}^C) + \lambda_{jC} N_{r,j}^C - \kappa_{jC} \cdot I_{r,1}^C + m_r \cdot Z_r + \varepsilon_{r,j}^C
\end{aligned} \tag{13}$$

$$\begin{aligned}
p_{r,j}^{G} &= \mathbf{u}_r^G \cdot \psi(t,t_0)^G \cdot \mathbf{o}_0{}^G - t^G + t_r + c(d_{rG,j} - d_j{}^G) + \kappa_{jG} \cdot I_{r,1}^G + m_r \cdot Z_r + e_{r,j}^G \\
p_{r,j}^{R_k} &= \mathbf{u}_r^R \cdot \psi(t,t_0)^R \cdot \mathbf{o}_0{}^R - t^R + t_r + c(d_{rR_k,j} - d_j{}^R) + \kappa_{jR_k} \cdot I_{r,1}^R + m_r \cdot Z_r + e_{r,j}^R \\
p_{r,j}^{E} &= \mathbf{u}_r^E \cdot \psi(t,t_0)^E \cdot \mathbf{o}_0{}^E - t^E + t_r + c(d_{rE,j} - d_j{}^E) + \kappa_{jE} \cdot I_{r,1}^E + m_r \cdot Z_r + e_{r,j}^E \\
p_{r,j}^{C} &= \mathbf{u}_r^C \cdot \psi(t,t_0)^C \cdot \mathbf{o}_0{}^C - t^C + t_r + c(d_{rC,j} - d_j{}^C) + \kappa_{jC} \cdot I_{r,1}^C + m_r \cdot Z_r + e_{r,j}^C
\end{aligned} \tag{14}$$

The POD parameters to be estimated in the combined mode contain initial orbit state $\mathbf{o}_0{}^s$, satellite clock bias t^s, receiver clock bias t_r, zenith tropospheric wet delay Z_r, phase ambiguities N_r^s, and the system/frequency dependent code biases in the receiver end, i.e. d_{rR_k}, d_{rE} and d_{rC} relative to the GPS biases d_{rG}. In principle, raw-observation model with appropriate ionospheric constraints can improve the POD performance. However, the POD procedure usually requires about one hundred or more stations, the estimation of epoch-wise ionospheric delay parameters for each station-satellite pair will introduce a huge number of additional parameters, which are even more than the sum of all other parameters. In order to achieve the balance between computation efficiency and optimal model, we apply the ionosphere-free linear combination for rapid POD in real-time applications. The ionospheric delays $I_{r,1}^s$ are eliminated, the ionosphere-free code biases d_{rG} and d^s are set to zero and will be absorbed by clock parameters t_r and t^s, respectively. The phase delays b_r and b^s will be absorbed by phase ambiguities parameters. Then, the estimated parameters are expressed as,

$$X = \left(\mathbf{o}_0{}^s \; \bar{t}^s \; \bar{t}_r \; Z_r \; d_{rE} \; d_{rC} \; d_{rR_k} \; \bar{N}_r^s \right)^T \tag{15}$$

$$
\begin{aligned}
\bar{t}^{s} &= t^{s} + d^{s} \\
\bar{t}_{r} &= t_{r} + d_{rG} \\
\bar{N}_{r}^{s} &= N_{r}^{s} + b_{r} + b^{s}
\end{aligned}
\tag{16}
$$

The real-time orbit is usually predicted based on orbits determined in a batch-processing mode using the latest available observations due to the dynamic stability of the satellite movement. More challenging is the estimation of the satellite clock corrections, which must be updated much more frequently due to their short-term fluctuations (Zhang et al., 2011). During clock estimation, the satellite orbit and station coordinates are held fixed (or tightly constrained),

$$
\begin{aligned}
l_{r,j}^{G} &= -t^{G} + t_{r} + \lambda_{jG}(b_{rG,j} - b_{j}^{G}) + \lambda_{jG} N_{r,j}^{G} - \kappa_{jG} \cdot I_{r,1}^{G} + m_{r} \cdot Z_{r} + \varepsilon_{r,j}^{G} \\
l_{r,j}^{R_k} &= -t^{R} + t_{r} + \lambda_{jR_k}(b_{rR_k,j} - b_{j}^{R}) + \lambda_{jR_k} N_{r,j}^{R} - \kappa_{jR_k} \cdot I_{r,1}^{R} + m_{r} \cdot Z_{r} + \varepsilon_{r,j}^{R} \\
l_{r,j}^{E} &= -t^{E} + t_{r} + \lambda_{jE}(b_{rE,j} - b_{j}^{E}) + \lambda_{jE} N_{r,j}^{E} - \kappa_{jE} \cdot I_{r,1}^{E} + m_{r} \cdot Z_{r} + \varepsilon_{r,j}^{E} \\
l_{r,j}^{C} &= -t^{C} + t_{r} + \lambda_{jC}(b_{rC,j} - b_{j}^{C}) + \lambda_{jC} N_{r,j}^{C} - \kappa_{jC} \cdot I_{r,1}^{C} + m_{r} \cdot Z_{r} + \varepsilon_{r,j}^{C}
\end{aligned}
\tag{17}
$$

$$
\begin{aligned}
p_{r,j}^{G} &= -t^{G} + t_{r} + c(d_{rG,j} - d_{j}^{G}) + \kappa_{jG} \cdot I_{r,1}^{G} + m_{r} \cdot Z_{r} + e_{r,j}^{G} \\
p_{r,j}^{R_k} &= -t^{R} + t_{r} + c(d_{rR_k,j} - d_{j}^{R}) + \kappa_{jR_k} \cdot I_{r,1}^{R} + m_{r} \cdot Z_{r} + e_{r,j}^{R} \\
p_{r,j}^{E} &= -t^{E} + t_{r} + c(d_{rE,j} - d_{j}^{E}) + \kappa_{jE} \cdot I_{r,1}^{E} + m_{r} \cdot Z_{r} + e_{r,j}^{E} \\
p_{r,j}^{C} &= -t^{C} + t_{r} + c(d_{rC,j} - d_{j}^{C}) + \kappa_{jC} \cdot I_{r,1}^{C} + m_{r} \cdot Z_{r} + e_{r,j}^{C}
\end{aligned}
\tag{18}
$$

To ensure the rapid update of real-time clock corrections (e.g., five seconds for IGS Real-time Pilot Project, RTPP), the ionosphere-free model is also applied in PCE procedure to eliminate ionospheric parameters. Meanwhile, code biases that are computed from previous day or POD procedure are introduced as known values to further reduce the number of estimated parameters. The satellite clock corrections obtained in a combined analysis of the multi-GNSS observations refer to one and the same reference clock assessed via GPS measurements in the network solution. The estimated parameters are expressed as,

$$
X = \left(\bar{t}^{s} \; \bar{t}_{r} \; Z_{r} \; \bar{N}_{r}^{s} \right)^{T}
\tag{19}
$$

The time-consuming network solution must be used for the estimation of precise satellite orbits and precise clocks. If in the case of post-processing, it will be possible to use raw-observation model for POD and PCE, then DCB and ionospheric products can also be derived together with orbit and clock products in one common parameter estimation procedure.

With satellite orbit, clock and DCB corrections, the corresponding terms in the observation equations can be removed and the PPP model can be expressed as,

$$
\begin{aligned}
l_{r,j}^{G} &= -\mathbf{u}_r^{G}\cdot\mathbf{r}_r + t_r + \lambda_{jG}(b_{rG,j} - b_j^{G}) + \lambda_{jG}N_{r,j}^{G} - \kappa_{jG}\cdot I_{r,1}^{G} + m_r\cdot Z_r + \varepsilon_{r,j}^{G}\\
l_{r,j}^{R_k} &= -\mathbf{u}_r^{R}\cdot\mathbf{r}_r + t_r + \lambda_{jR_k}(b_{rR_k,j} - b_j^{R}) + \lambda_{jR_k}N_{r,j}^{R} - \kappa_{jR_k}\cdot I_{r,1}^{R} + m_r\cdot Z_r + \varepsilon_{r,j}^{R}\\
l_{r,j}^{E} &= -\mathbf{u}_r^{E}\cdot\mathbf{r}_r + t_r + \lambda_{jE}(b_{rE,j} - b_j^{E}) + \lambda_{jE}N_{r,j}^{E} - \kappa_{jE}\cdot I_{r,1}^{E} + m_r\cdot Z_r + \varepsilon_{r,j}^{E}\\
l_{r,j}^{C} &= -\mathbf{u}_r^{C}\cdot\mathbf{r}_r + t_r + \lambda_{jC}(b_{rC,j} - b_j^{C}) + \lambda_{jC}N_{r,j}^{C} - \kappa_{jC}\cdot I_{r,1}^{C} + m_r\cdot Z_r + \varepsilon_{r,j}^{C}
\end{aligned}
\tag{20}
$$

$$
\begin{aligned}
p_{r,j}^{G} &= -\mathbf{u}_r^{G}\cdot\mathbf{r}_r + t_r + c\cdot\kappa_j\cdot d_{rG,1} + \kappa_{jG}\cdot I_{r,1}^{G} + m_r\cdot Z_r + e_{r,j}^{G}\\
p_{r,j}^{R_k} &= -\mathbf{u}_r^{R}\cdot\mathbf{r}_r + t_r + c\cdot\kappa_j\cdot d_{rR_k,1} + \kappa_{jR_k}\cdot I_{r,1}^{R} + m_r\cdot Z_r + e_{r,j}^{R}\\
p_{r,j}^{E} &= -\mathbf{u}_r^{E}\cdot\mathbf{r}_r + t_r + c\cdot\kappa_j\cdot d_{rE,1} + \kappa_{jE}\cdot I_{r,1}^{E} + m_r\cdot Z_r + e_{r,j}^{E}\\
p_{r,j}^{C} &= -\mathbf{u}_r^{C}\cdot\mathbf{r}_r + t_r + c\cdot\kappa_j\cdot d_{rC,1} + \kappa_{jC}\cdot I_{r,1}^{C} + m_r\cdot Z_r + e_{r,j}^{C}
\end{aligned}
\tag{21}
$$

PPP, as a single-receiver technique, is very efficient even if ionospheric parameters are estimated. Therefore, we adopt the raw-observation model with ionospheric constraints of equation (6) to improve the PPP performance. The estimated parameters are,

$$X = \left(\mathbf{r}_r\ \bar{t}_r\ Z_r\ d_{r,1}\ I_{r,1}^{s}\ \bar{N}_r^{s}\right)^T \tag{22}$$

In multi-GNSS PPP, ISB and IFB parameters have to be estimated or corrected from well-known values. If UPD and ionospheric products are also available, rapid ambiguity resolution then can be achieved (Li et al., 2013b).

3.4 Data processing strategy

Because of the same ranging and positioning principle for different GNSS, most of the observational error models and satellite force models for GPS can be utilized directly for other systems, i.e. GLONASS, Galileo and BeiDou. However, some modifications in the multi-GNSS processing were necessary due to different frequencies, additional parameters (e.g. ISB) and in particular due to different characteristics of the BeiDou orbits (e.g. satellite attitude control mechanics, constellation distribution, maneuver detection and handling). Table 4 summarized our multi-GNSS data processing strategy, observation models and estimated parameters for POD, PCE, and PPP.

All observations of four systems (~74 satellites) from IGS+MGEX+BETN network (about 120 stations) are analyzed using an integrated processing mode with one common parameter estimation. Considering computation efficiency for rapid update of real-time orbit and clock, ISB/IFB products derived from previous day of post-processing are introduced as known values to reduce the number of estimated parameters and ionosphere-free linear combination is used to eliminate ionospheric parameters in network solution. For PPP at user end, ISB, IFB and ionospheric parameters are estimated. Double-differenced ambiguity resolution (AR) is implemented as a standard processing for network solution. Undifferenced ambiguity resolution can be performed as an optional strategy when UPD product is available.

Table 4. Multi-GNSS data processing strategy, observation models and estimated parameters for POD, PCE, and PPP

Item	Models
Satellites	BeiDou+Galileo+GLONASS+GPS; about 74 satellites
Procedure	Integrated processing, all the observations from different GNSS in one common parameter adjustment procedure
Estimator	LSQ in batch mode for POD; LSQ in sequential mode for PCE & PPP
Observations	Undifferenced phase and code observations
Combination mode	Ionosphere-free combination for POD/PCE network solution; raw observations on individual frequencies for PPP
Signal selection	GPS: L1/L2; GLONASS: L1/L2; BeiDou: B1/B2; Galileo: E1/E5a
Tracking data	IGS+MGEX+BETN (about 120 stations) for POD and PCE; Local CORS and some MGEX stations are selected for PPP
Sampling rate	30s
Elevation cutoff	7°
Observation weight	Elevation dependent weight
Phase-windup effect	Corrected
Earth rotation parameter	Estimated with tight constraint (He et al., 2013b)
Tropospheric delay	Initial model + random-walk process
Ionospheric delay	Eliminated by ionosphere-free combination in POD and PCE; estimated as parameters in PPP
Receiver clock	Estimated, white noise
ISB and IFB	Estimated as constant with zero mean conditions in post-processing; introduced as known values in real-time
Station displacement	Solid Earth tide, pole tide, ocean tide loading, IERS Convention 2003 (McCarthy and Petit, 2003)
Satellite antenna phase center	Corrected using MGEX and IGS values
Receiver antenna phase center	Corrected using GPS values
Terrestrial frame	ITRF2008 (Altamimi et al., 2011)
Satellite orbit	Estimated in POD; Fixed in PCE&PPP using the products from POD
Satellite clock	Estimated in POD and PCE, white noise; Fixed in PPP using the products from PCE
Station coordinate	Fixed (or tightly constrained) in POD and PCE; Estimated in epoch-wise kinematic mode for PPP
Phase ambiguities	Constant for each arc; Double-differenced AR for network solution, undifferenced AR if UPD available

The dynamical models involved for multi-GNSS POD are listed in Table 5. POD and PCE are essential functions of precise positioning service and their performance in terms of accuracy and time latency decides somehow the capacity of the system services. In order to obtain a stable solution, long data arcs (three-day solution) are used for POD because of the weak observing geometry of BeiDou and Galileo due to the constellation, number of satellites and limited ground tracking network. Especially for BeiDou system, GEO satellites have almost no movement with respect to the ground network and IGSOs are restricted within a certain longitude zone. Therefore, long arc estimation is very important for current BeiDou constellation. In this contribution, we use three-day data in a batch estimation to obtain a three-day solution, instead of combining three daily solutions on the level of normal equations. Meanwhile, velocity breaks are introduced every 12 hours. BeiDou applies different attitude mode compared to GPS, yaw-fixed attitude mode is used for GEO satellites and nominal attitude with yaw maneuver for MEO and IGSO satellites.

Table 5. Dynamical models involved for multi-GNSS POD.

Item	**Models**
Orbit arc	3-day solution
Geopotential	EGM96 model (12×12)
Tide	Solid Earth tide, pole tide, ocean tide IERS Conventions 2003
M-body gravity	Sun, Moon and all planets (JPL DE405)
Solar Radiation Pressure	Bern five parameters with no initial value
Relativistic Effect	Applied
Velocity breaks	Every other 12 hours
Attitude model	Nominal attitude for GPS/GLONASS/Galileo; Nominal attitude with yaw maneuver for MEO and IGSO satellites of BeiDou; Yaw-fixed attitude mode used for GEO satellites of BeiDou

3.5 Prototype Multi-GNSS Real-time Precise Positioning Service

High-precision (centimeter level) real-time positioning is expected to benefit significantly in terms of precision, reliability, availability and convergence from the development of new global and regional navigation satellite systems. Therefore, GFZ, which is operationally providing GPS orbits, clocks, and UPDs for real-time PPP service, recently put much effort on promoting its real-time service for multi-GNSS applications. The structure of our prototype multi-GNSS real-time PPP system is shown in Fig. 4.

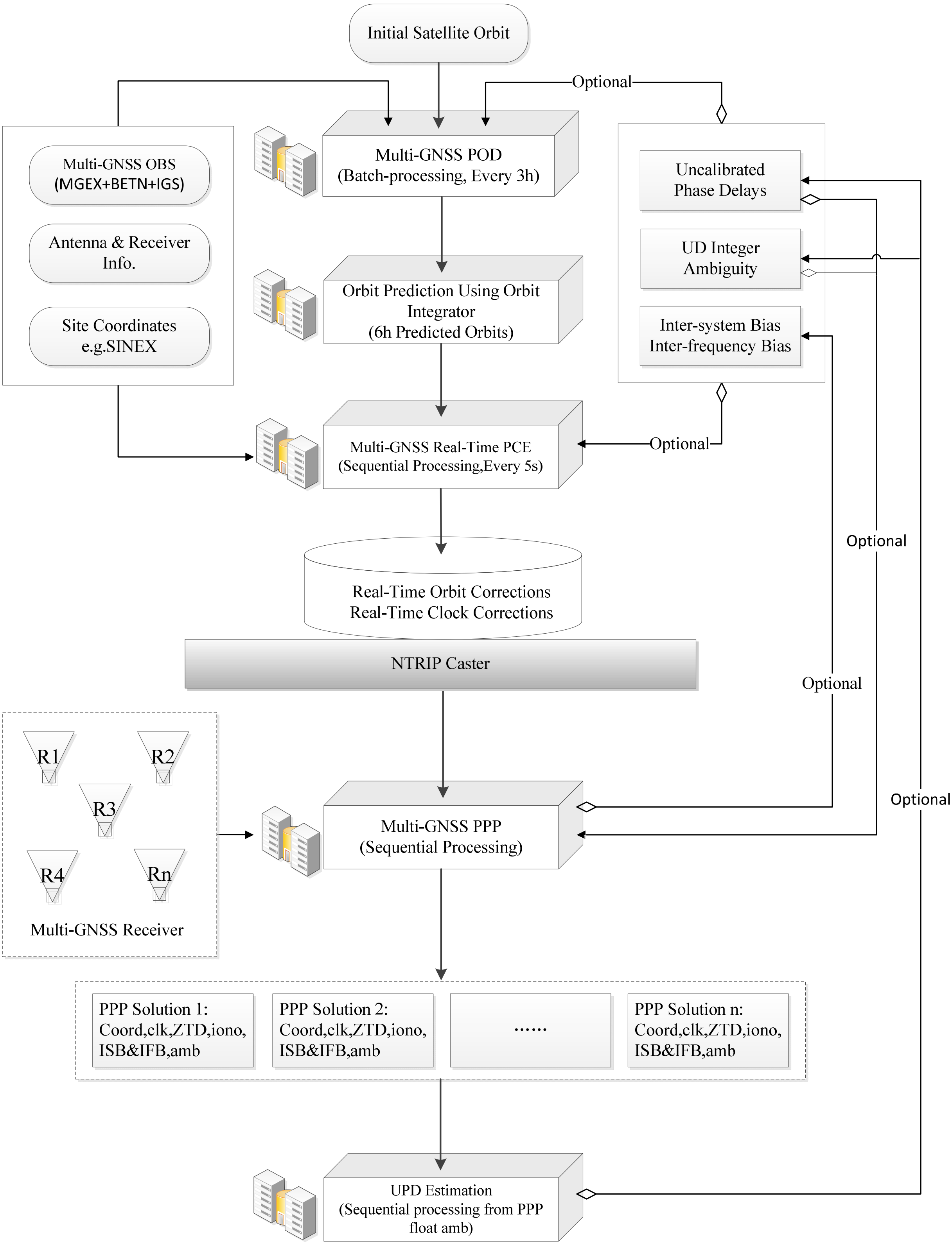

Figure 4. The structure of the prototype multi-GNSS real-time PPP service system at GFZ.

In a global real-time PPP service system, real-time data from a global reference network with a certain number of evenly distributed stations is essential for generating precise orbits and clocks for precise positioning at the desired location. Under the framework of the IGS RTPP, GPS data from a global real-time network of more than 100 stations is available and the related data communication for the observation, retrieving and product casting was established (Caissy et al., 2012). Meanwhile, a large subset of MGEX stations also provides real-time data streams with multi-GNSS observations to the MGEX project. BKG, Frankfurt, hosts a dedicated online caster (http://mgex.igs-ip.net) for the MGEX project, where interested users can presently access data streams from roughly 70 stations following a free registration (Montenbruck et al., 2014). However, the BeiDou data of BETN are not available in real-time at the moment. Therefore, we run the multi-GNSS precise positioning service system in simulated real-time mode for this demonstration.

Firstly, multi-GNSS POD is carried out in batch-processing mode using the observations from MGEX+BETN+IGS networks. In order to ensure the rapid orbit update of every three hours, we try to minimize the number of the estimated parameters by fixing the ISB&IFB to the values derived from previous day of post-processing and fixing site coordinates to SINEX (or weekly) solution instead of strong constraints. In addition, POD on undifferenced integer ambiguity level is achievable if uncalibrated phase delay products are available and applied. Even when undifferenced integer ambiguities are also available from PPP fixed solutions of all stations or UPD estimation, all of the fixed ambiguities can be removed from parameter estimation and the number of estimated parameters can be further reduced.

The real-time orbit is predicted (here six hours prediction) based on the orbits determined in a batch-processing mode by using orbit integrator. The satellite clock corrections must be updated much more frequently due to their short-term fluctuations, e.g., five seconds sampling interval is adopted in RTPP. The rapid generation of clock corrections is especially challenging in multi-GNSS processing because of more observations and more parameters are included. Therefore, in our clock estimation, not only satellite orbits but also site coordinates and ISB&IFB are fixed to well-known values. The satellite clocks are estimated together with receiver clocks, ambiguities and zenith tropospheric delays. Table 6 lists the number of estimated parameters in multi-GNSS real-time clock estimation. When all the parameters except orbits are estimated, the total number of estimated parameters at each epoch will reach up to about 6,434 and the processing time will be about 30 s. Such a long process time, of course, cannot satisfy the requirement of rapid clock update (e.g. 5 s). Fortunately, if we fix site coordinates and ISB&IFB to well-known values and do not estimate horizontal gradients, the total number of estimated parameters at each epoch is reduced to about 2,714 and the process time is significantly decreased to about 2 s, which can satisfy the clock update of 5 s sampling interval.

Similar to the POD procedure, if UPD and undifferenced integer ambiguities are also available, the ambiguity parameters can also be removed from clock estimation. The number of estimated parameters will be further reduced to only about 314 and the process time is much less than 1 s, which will be very useful when much more observations are available and much more parameters have to be estimated in the future as the further development of multi-GNSS.

Table 6. The number of estimated parameters in multi-GNSS real-time clock estimation

Parameters/Number	**Estimate all**	**Rapid update**	**Fix ambiguity**
Satellite clocks	~74	~74	~74
Receiver clocks	~120	~120	~120
Tropospheric delays	~120	~120	~120
Horizontal gradient	~120*2	0	0
Site coordinates	~120*3	0	0
Ambiguities	~120*20	~120*20	0
Inter-system biases	~120*2	0	0
Inter-frequency biases	~120*24	0	0
Sum	~6434	~2714	~314
Process time	~30s	~2s	<<1s

With the real-time orbit and clock corrections from service caster, multi-GNSS PPP can be carried out at the user-end. The estimated parameters include site coordinates, receiver clock, zenith tropospheric delays, ionospheric parameters, ISB&IFB and float ambiguities. Based on the float ambiguities derived from PPP solutions, UPD can be estimated in real time and transmitted to service caster. Once UPD products are available, undifferenced ambiguity resolution is straightforward in PPP as well as POD and PCE.

The prototype multi-GNSS real-time PPP system, which was developed in this contribution at GFZ, is based on the Position and Navigation Data Analyst (PANDA, Liu and Ge, 2003) and iPPP (Li et al., 2011) software. It is used for the simulated real-time demonstration and will be implemented in the EPOS-RT software (Ge et al. 2012, Li et al., 2013a) for an operational multi-GNSS real-time service.

4 Accuracy and reliability of Multi-GNSS

4.1 Orbit and clock quality

The MGEX+BETN+IGS networks including stations all over the world provide an excellent opportunity for experimental studies to demonstrate the performance of the above described real-time processing system. Precise orbit determination and clock estimation are essential prerequisites of precise positioning service and their performance in terms of accuracy and time latency decides somehow the capacity of the system services. In order to assess the precision of orbit and clock solutions, we processed three months' data of September, October (day of year from 244 to 305) in 2013 and March (day of year from 60 to 90) in 2014 in the four-system integrated mode. These two time periods were selected because of the availability of the BETN data.

The quality of POD is assessed as usual by the orbit consistency of two adjacent three-day solutions during the overlapping interval: the orbit of the last two days in one three-day solution is compared with that of the first two days in the next. For any two adjacent 3-day solutions shifted by 1 day, there are 48 h overlapping orbit positions. We use this 48 h overlaps to evaluate the internal consistency of our orbit solutions. Figure 5 shows the averaged RMS (root mean square) values of 48 h overlap in along-track, cross-track and radial component for each satellite.

For the GPS satellites, the overlap RMS values are generally better than 1 cm in radial and cross-track directions, and better than 2 cm in along-track direction. The averaged RMS values of all GPS satellites are 0.7, 0.8, and 1.5 cm in radial, cross-track and along-track components, respectively. The achieved accuracy is comparable to the IGS final solutions (Dow et al., 2009). For the GLONASS satellites, the averaged RMS values are 1.3, 2.3, and 4.3 cm in radial, cross-track and along-track components, respectively. It is slightly worse than GPS orbit accuracy due to the difficulty in GLONASS ambiguity resolution (float ambiguities here for GLONASS). The orbit accuracy of Galileo is 2.1, 3.7 and 7.8 cm respectively in radial, cross-track and along-track components, which is worse than both GPS and GLONASS. It can be caused by limited available satellites (only four MEOs) and limited number of ground tracking stations.

For IGSO satellites of BeiDou, the overlap RMS values are generally better than 5 cm in all three components, the averaged RMS values of five IGSO satellites are 2.5, 3.3, and 4.4 cm in radial, cross-track and along-track components, respectively. It is comparable to the Galileo results. For the four MEO satellites, the averaged RMS values are respectively 3.4 and 4.3 cm in the radial and cross-track directions, a little worse than IGSO. The RMS values in the along-track direction are obviously increased to 11.3 cm. The GEO satellites have similar performance with IGSO and MEO satellites in the radial and cross-track directions, which are 4.8 and 2.8 cm, respectively. However, the accuracy of the along-track component is significantly decreased to about 90 cm.

Table 7 shows the averaged RMS values of the 48 h overlaps in along-track, cross-track and radial component for all orbital types. It can be seen that the RMS values of along-track component for all the satellites are the largest among the three components. Furthermore, the along-track RMS values for GEO are much larger than those of IGSO and MEO. The reason for this phenomenon is that GEO satellites do not move significantly in the along-track component with respect to the ground stations, resulting in rather weak geometrical constellation. It should be mentioned that the GNSS observations of positioning users at the Earth surface are less sensitive to errors of the along- and cross-track orbit components than those of the radial one, therefore the errors in the along- and cross-track components may have a less significant impact on the quality of the user positioning. Moreover, these errors (i.e., differences) are almost a constant over a long period. The projection of along-track errors in the line-of-sight can be effectively absorbed by ambiguity terms in user positioning.

Parameter differences over the overlapping time of two adjacent three-day solutions are also utilized to assess the quality of the estimated clocks. The RMS of the clock differences is taken as clock quality indicator. The mean biases are removed as they can be absorbed by ambiguity items and will not affect user positioning. It means that the RMS here is equal to standard derivation. Figure 6 shows the averaged RMS values for each satellite. For GPS satellites, the overlap RMS values are generally better than 0.1 ns. The averaged RMS values of all GPS satellites are 0.034 ns. The GLONASS clock accuracy is worse than GPS with a RMS value of 0.066 ns. The Galileo and BeiDou clocks can achieve comparable accuracy to GLONASS clocks, which are 0.066 and 0.065 ns, respectively. The relatively large clock overlaps for Galileo may be caused by the sparse amount of available tracking data. Although the GEO orbits are worse than other satellite types, the corresponding clock accuracy is also generally better than 0.1 ns as the satellite clocks are mainly correlated with the radial orbit component.

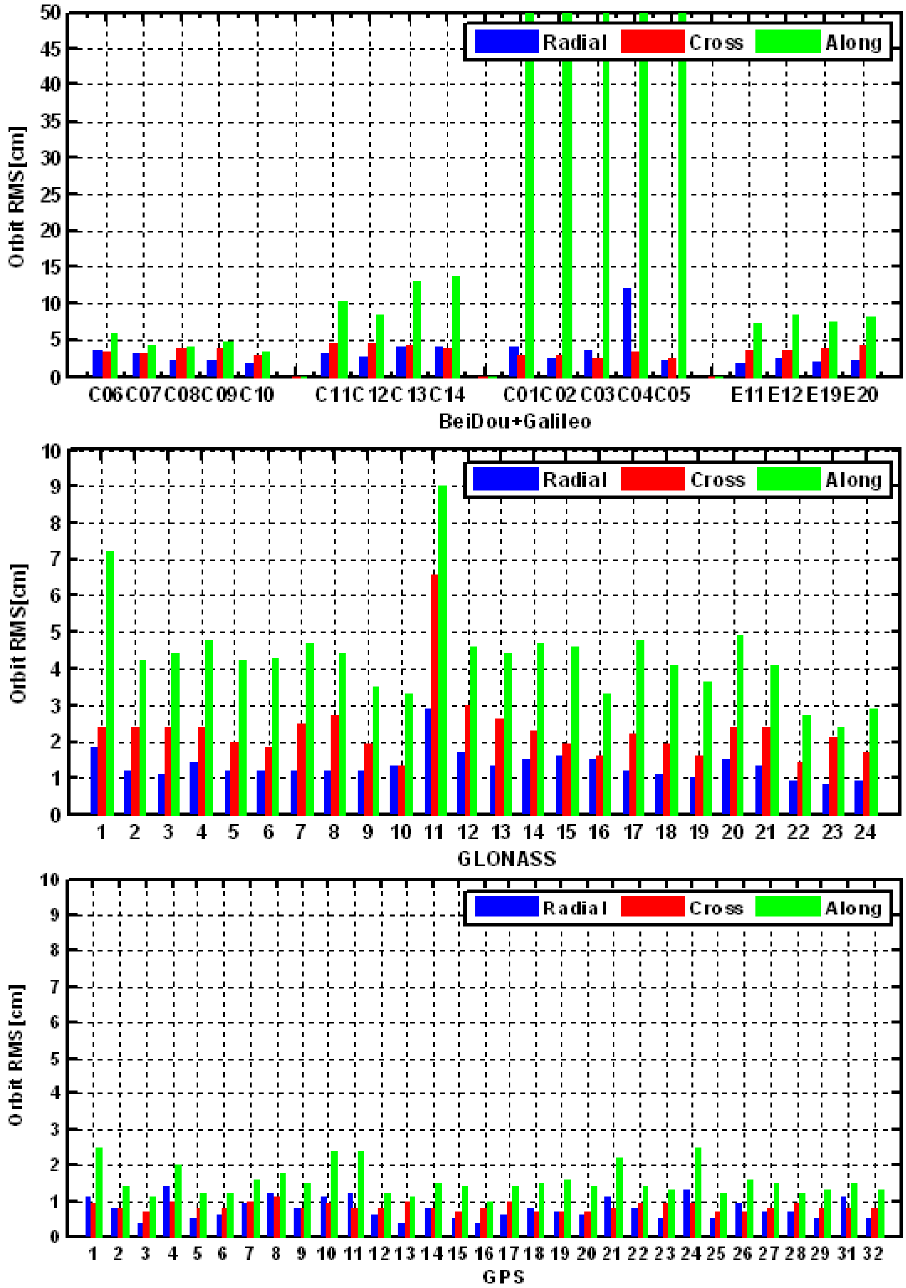

Figure 5. Averaged RMS values of 48 h orbit overlap differences in radial, cross, and along directions for BeiDou (top sub-figure), Galileo (top sub-figure), GLONASS (middle sub-figure) and GPS (bottom sub-figure).

Table 7. The averaged RMS values of 48-h overlap in along- (A), cross-track (C) and radial (R) components.

Satellite	**R(cm)**	**C(cm)**	**A(cm)**	**3D(cm)**
BeiDou IGSO	2.5	3.3	4.4	6.0
BeiDou MEO	3.4	4.3	11.3	12.5
BeiDou GEO	4.8	2.8	90.8	90.9
Galileo	2.1	3.7	7.8	8.8
GLONASS	1.3	2.3	4.3	5.0
GPS	0.7	0.8	1.5	1.8

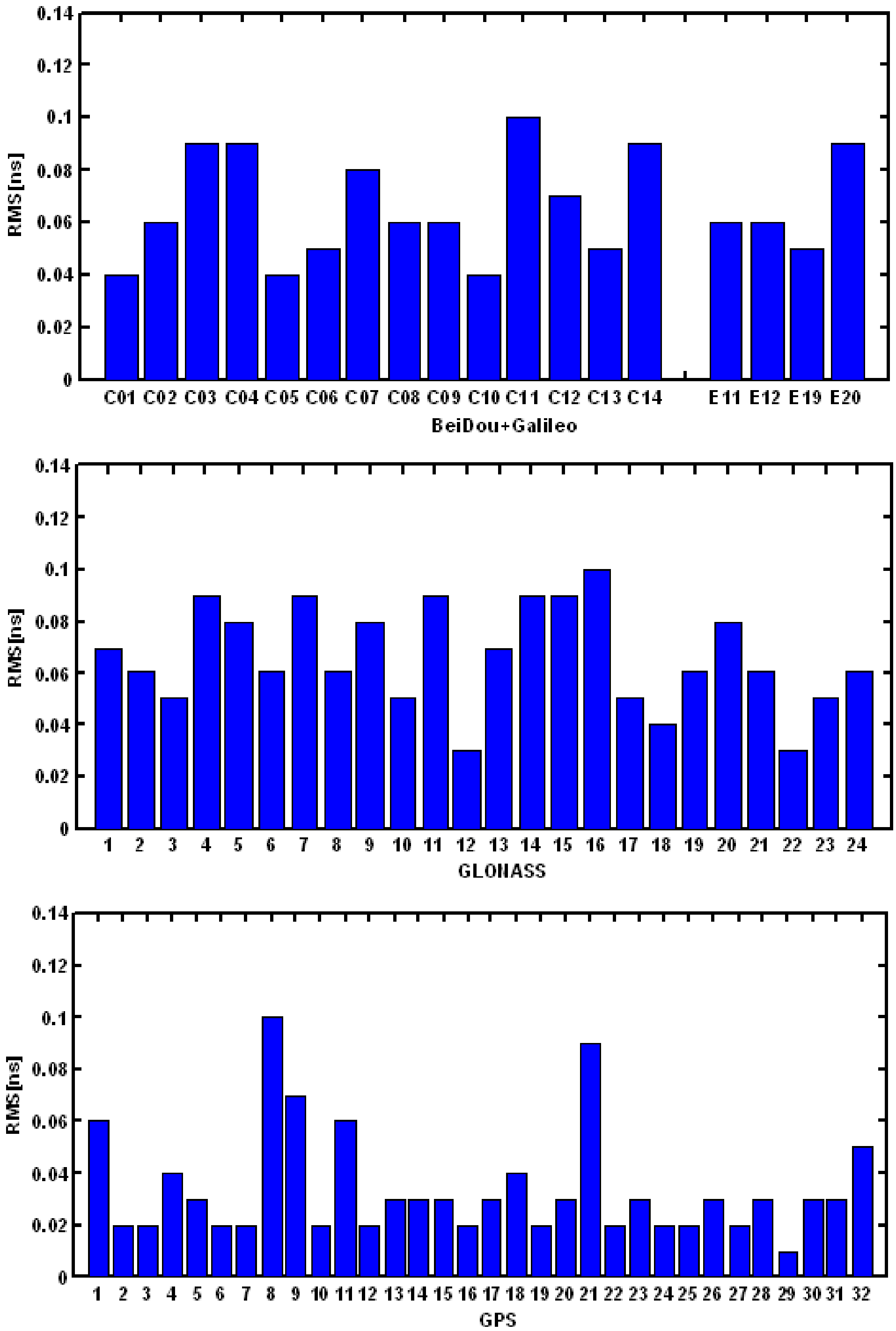

Figure 6. Averaged RMS values of 48h clock overlap differences for BeiDou (top sub-figure), Galileo (top sub-figure), GLONASS (middle sub-figure) and GPS (bottom sub-figure).

Because of the dynamic stability of the satellite movement, the real-time orbit is usually predicted based on orbits determined in a batch-processing mode using the latest available observations, e.g. the

IGS ultra-rapid orbits. We use estimates of the three-day POD solution as base to predict the orbits of 6 hours after. The predicted orbits are compared with the corresponding hours of the middle day in a 3-day solution to assess the accuracy of predicted real-time orbit. Figure 7 shows the averaged RMS values of orbit differences between the 6 h predicted and estimated ones in radial, cross-track, and along-track directions for each satellite.

The statistical accuracy of the 6 h predicted orbits for each satellite type is summarized in Table 8. It can be seen that the along-track component is still the worst of the three directions, especially for GEO satellites. However, the radial and cross RMS values are smaller than 10 cm for BeiDou and Galileo, and smaller than 5 cm for both GLONASS and GPS satellites, respectively. The predicted orbit accuracy is several centimeters worse than estimated orbit in general.

The satellite clock corrections must be estimated and updated much more frequently due to their short-term fluctuations. With the predicted orbit hold fixed, we estimate satellite clocks epoch-by-epoch in simulated real-time mode in which well-known station coordinates and ISB&IFB values are introduced. The precise clock products derived from batch-processing mode are used to assess the quality of the real-time estimated clocks. Figure 8 shows the averaged RMS values of clock differences between the real-time and batch-processed solutions for each satellite. The GPS clocks have the best accuracy of about 0.10 ns, while the statistical accuracy of BeiDou, Galileo and GLONASS are 0.13, 0.13 and 0.14 ns, respectively. The results confirm that both satellite orbits and clocks can achieve an accuracy at cm level in real-time. Furthermore, the high correlation between the radial orbit component and satellites clocks allows the orbital errors to be compensated by the clock estimation.

The quality of the BeiDou and Galileo products is expected to be improved in the future from a densified tracking network, availability of more accurate parameters of the space segments and more available satellites (Montenbruck et al., 2012).

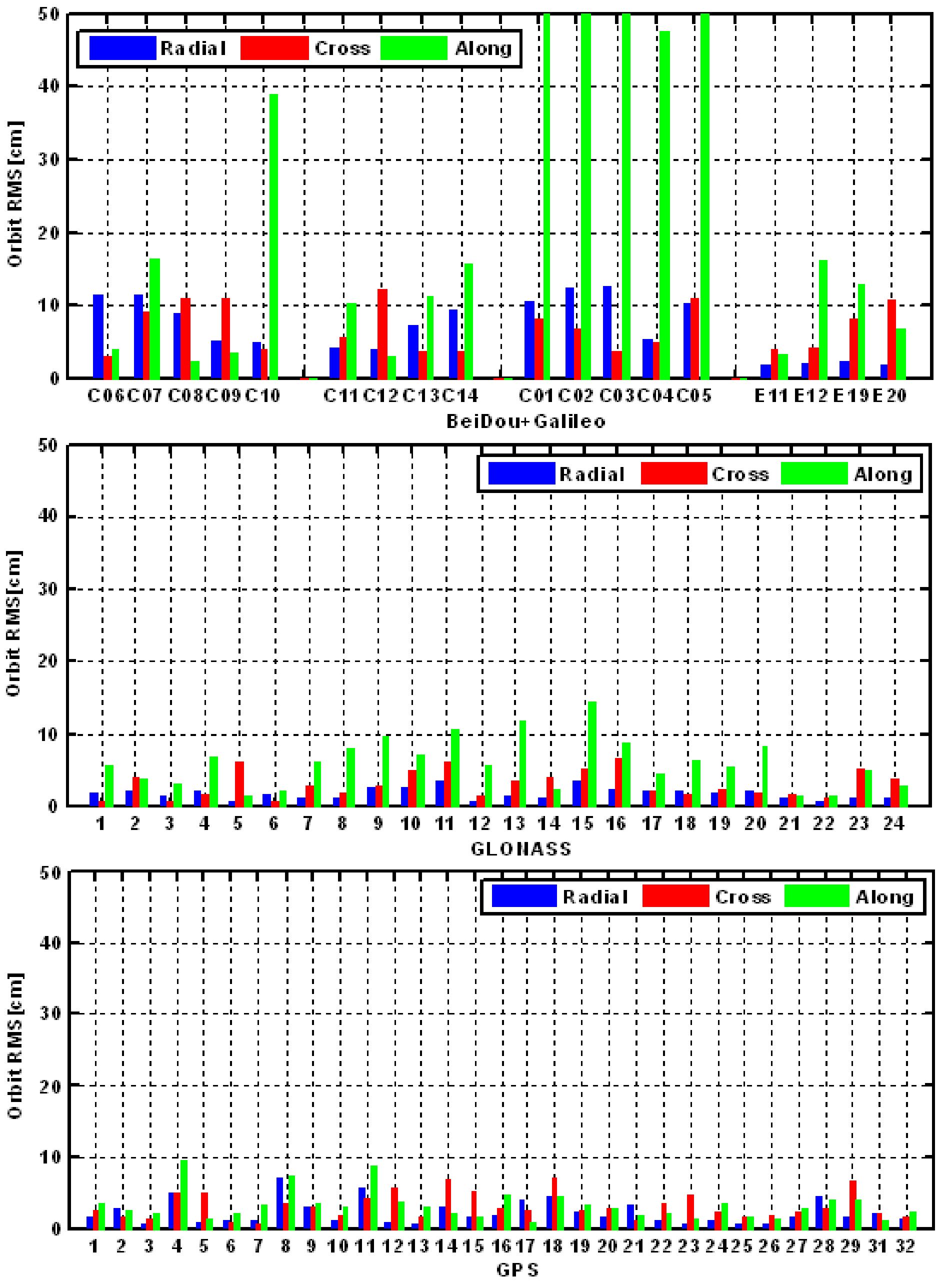

Figure 7. Averaged RMS values of orbit differences between the 6h predicted and estimated ones in radial, cross, and along directions for BeiDou (top sub-figure), Galileo (top sub-figure), GLONASS (middle sub-figure) and GPS (bottom sub-figure).

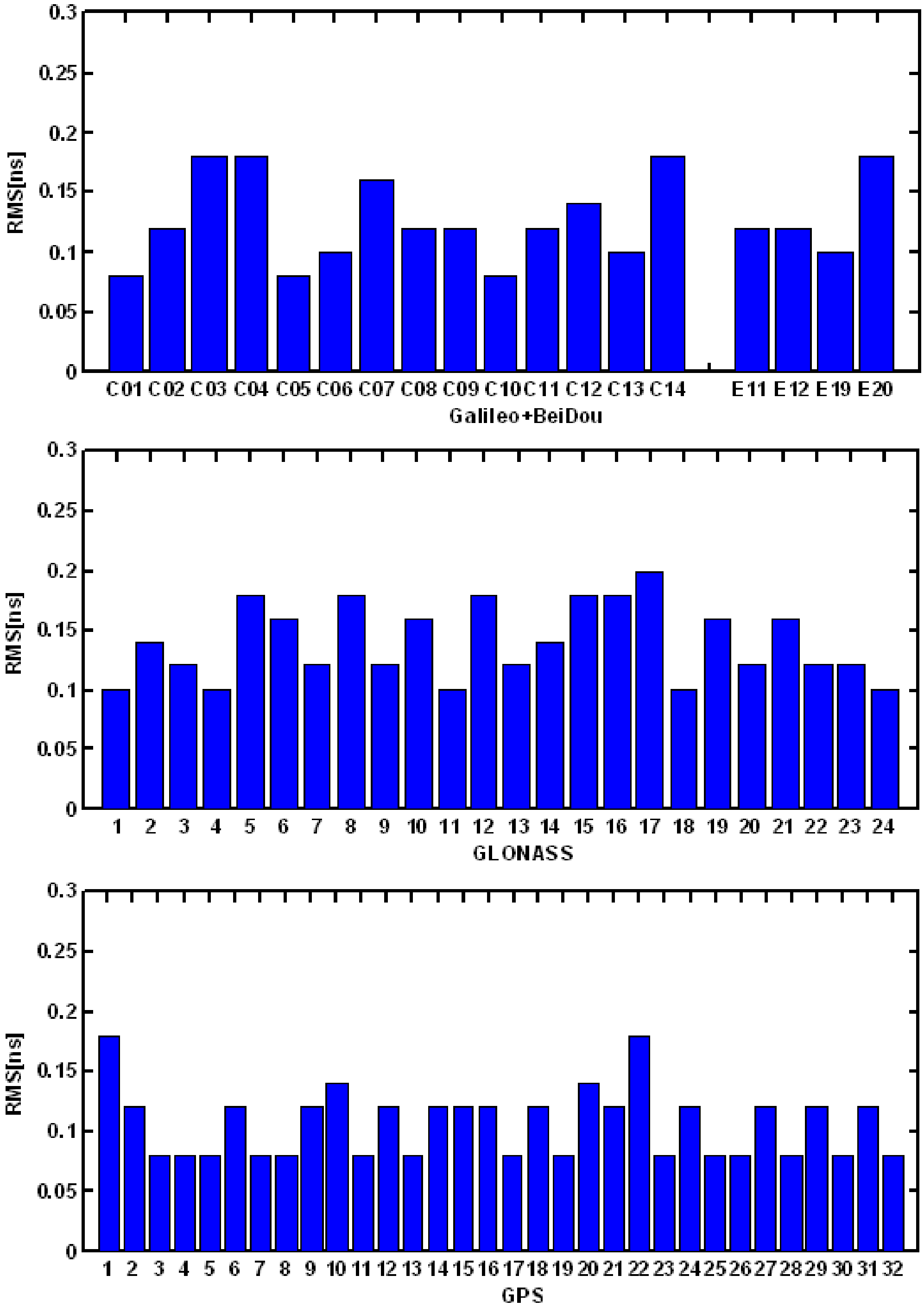

Figure 8. Averaged RMS values of clock differences between the real-time and post-processed ones for BeiDou (top sub-figure), Galileo (top sub-figure), GLONASS (middle sub-figure) and GPS (bottom sub-figure).

Table 8. The averaged RMS values of predicted orbit differences in along- (A), cross-track (C) and radial (R) components.

Satellite	R(cm)	C(cm)	A(cm)	3D(cm)
BeiDou IGSO	8.3	7.5	13.0	17.1
BeiDou MEO	6.3	6.2	12.0	14.9
BeiDou GEO	10.1	6.8	92.7	93.4
Galileo	2.9	6.8	9.8	12.2
GLONASS	2.2	3.1	5.9	7.0
GPS	1.8	3.0	3.2	4.7

4.2 Real-time kinematic PPP

Based on the predicted orbit and real-time estimated clocks, PPP can be performed to validate the capability of real-time precise positioning service. In this section, we select sixteen multi-GNSS stations as user end to analyze the performance of multi-GNSS PPP solutions. When one station is processed in PPP mode, it is excluded from service-end orbit and clock product generation so that the PPP solutions are independent. Four stations, CENT, CHDU, HKTU and SIGP, are equipped with the same dual-system receiver (GPS+BeiDou), while all the other stations are four-system receivers. All these data are processed both in single-system and combined modes. All the estimated station coordinates are compared with the SINEX or weekly solution.

In the PPP processing, satellite orbits and clocks are fixed to the abovementioned estimates. Receiver clock is estimated epoch-wise, remaining zenith tropospheric delay after an a priori model correction is parameterized with a random-walk process. Both ISB and IFB parameters are estimated as constant. The positions are estimated as epoch-wise parameters by means of the sequential least square adjustment to simulate the real-time kinematic situation.

Figure 9 presents the real-time kinematic PPP results in modes of GPS-only, BeiDou-only and combined GPS/BeiDou for the dual-system Unicore receiver at station CENT, which is located in the middle of China, Asia with latitude of 30.52° and longitude of 114.35°. The PPP solutions on September 1, 2013 and the satellite numbers on that day are presented here as a typical example. For the GPS-only solution, after a convergence of about one hour, the horizontal positioning accuracy of better than 5 cm and vertical accuracy of better than 1 dm are generally achievable in real-time PPP mode. The BeiDou-only PPP takes a relatively long convergence time of about three hours. Afterwards, the accuracy stays on cm-level. Therefore, with the current BeiDou regional system, autonomous positioning using BeiDou-only is already possible and positioning accuracy of better than 1 dm is achievable in real-time PPP mode. For horizontal components, the BeiDou-only solutions are stably staying within ±5 cm, while the vertical component is within ±10 cm after the convergence period. It is observed that there is a spike in the GPS only solutions around 15:30 UTC. At that moment, there are only five satellites observed due to a tracking problem (this is likely due to the fact that this type of receiver gives the higher priority to the BeiDou satellites), see Figure 9d. However, this spike can be easily solved if multi-GNSS observations are used together, see the combined GPS/BeiDou PPP solution in Figure 9c. As Figure 9c shows, the GPS /BeiDou kinematic PPP converges much faster than both BeiDou-only and GPS-only kinematic PPP, in all the three components. As Figure 9d has shown, at least eight satellites can be seen at CENT in every epoch for BeiDou kinematic PPP and the satellite numbers of combined BeiDou and GPS positioning increase significantly and at least 15 satellites are available in every epoch. As a result, both positioning accuracy and convergence time are significantly improved by multi-GNSS observations. Combined PPP can achieve more accurate and stable position series than that of BeiDou-only and GPS-only solutions.

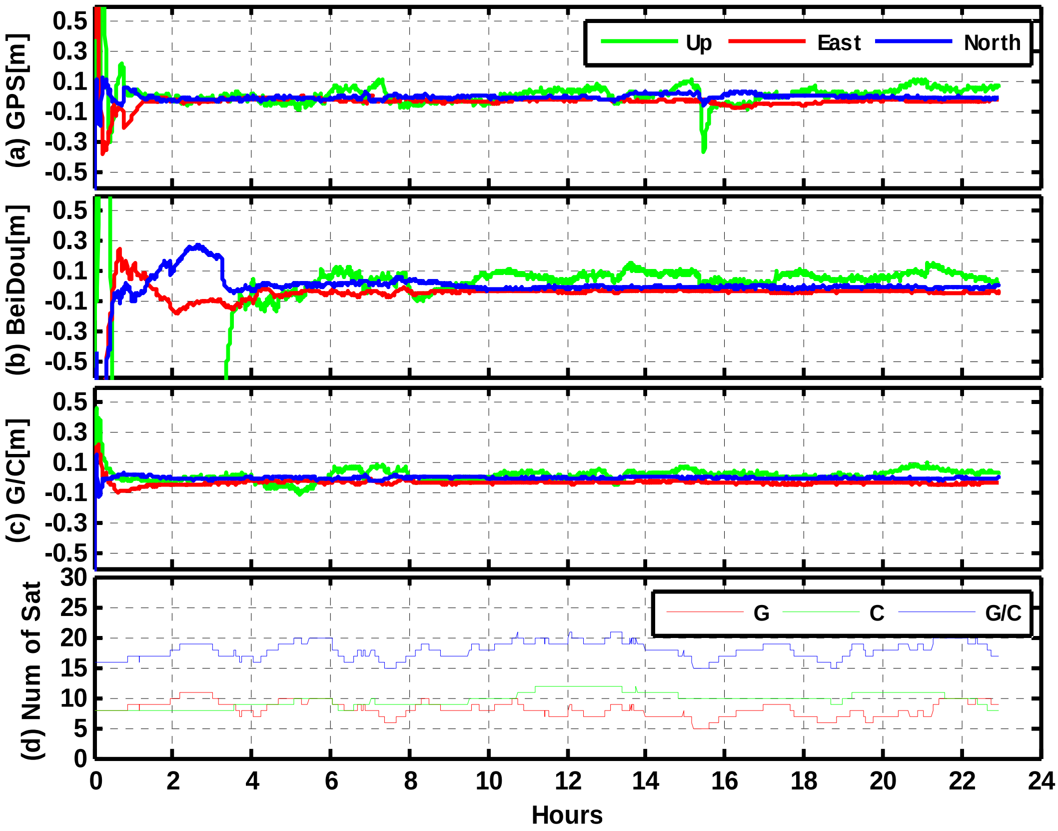

Figure 9. Comparisons of GPS, BeiDou and GPS/BeiDou kinematic PPP solutions at station CENT (latitude: 30.52°, longitude: 114.35°, China) on September 1, 2013

Figure 10 shows the kinematic PPP results in single-system, dual-system and four-system modes for the four-system Trimble R9 receiver at station CUT0, which is located in Australia with latitude of -32.00° and longitude of 115.89°. The left sub-figures show the single-system PPP results of GPS-only, BeiDou-only, GLONASS-only and Galileo-only, respectively. The GPS-only solution show similar performance with that of the station CENT. GLONASS can also provide autonomous positioning capability, however, the convergence of GLONASS-only PPP is relatively longer than GPS-only PPP, especially in north and up components. In addition, the GLONASS-only position series are slightly less stable than GPS results. Thanks to the distribution of the current BeiDou constellation, the CUT0 station in Australia has an excellent observational geometry for BeiDou and thus the Beidou-only PPP solution for this station can achieve very good performance especially in horizontal components, even better than that of CENT station which is in China. It is worth to notice that it is very likely that the high-grade Trimble R9 receiver has a higher quality than the Unicore receiver. It can be seen from this figure that the north component of BeiDou-only solution converges faster than the east and up components. The behavior is also the same for GPS-only solution. The north component of BeiDou-only kinematic solutions converge as fast as that of GPS-only while the east and up components converge more slowly than that of GPS-only. Galileo-only PPP solution cannot be achieved at the CUT0 station as only four satellites are currently in orbit.

The combined GPS/BeiDou，GPS/GLONASS，GPS/Galileo，GPS/BeiDou/GLONASS/Galileo kinematic PPP solutions are shown in right sub-figures. Obviously, the multi-GNSS combination significantly improves the PPP performance, compared to the left sub-figures of single-system solutions. The Galileo satellites have not contributed much to the combined GPS/Galileo PPP solution at this station because of limited Galileo observations. Figure 11 provides a more intuitive comparison of different PPP solutions in the east, north and up components, respectively. It can be clearly observed that the combined GPS/BeiDou and GPS/GLONASS solutions significantly shorten the convergence time and improve the position series compared to single-system PPP. The combined GPS+BeiDou+GLONASS+Galileo PPP presents fastest convergence and highest accuracy in all the three components, thanks to the increasing of satellite numbers and the improvement of the PDOP (positional dilution of precision) values, as shown in Figure 11d and 11e. About five to ten satellites can be seen at CUT0 in every epoch for GPS-only PPP and the variation PDOP is from 2 to 6. In contrast, the observed satellite numbers for multi-GNSS PPP with four systems are between 22 and 30 and the PDOP values are below 1.5 and very stable. Figure 12 shows the sky plots (azimuth vs elevation) of four systems at CUT0. The kinematic PPP results for some other stations are also shown in the Appendix I.

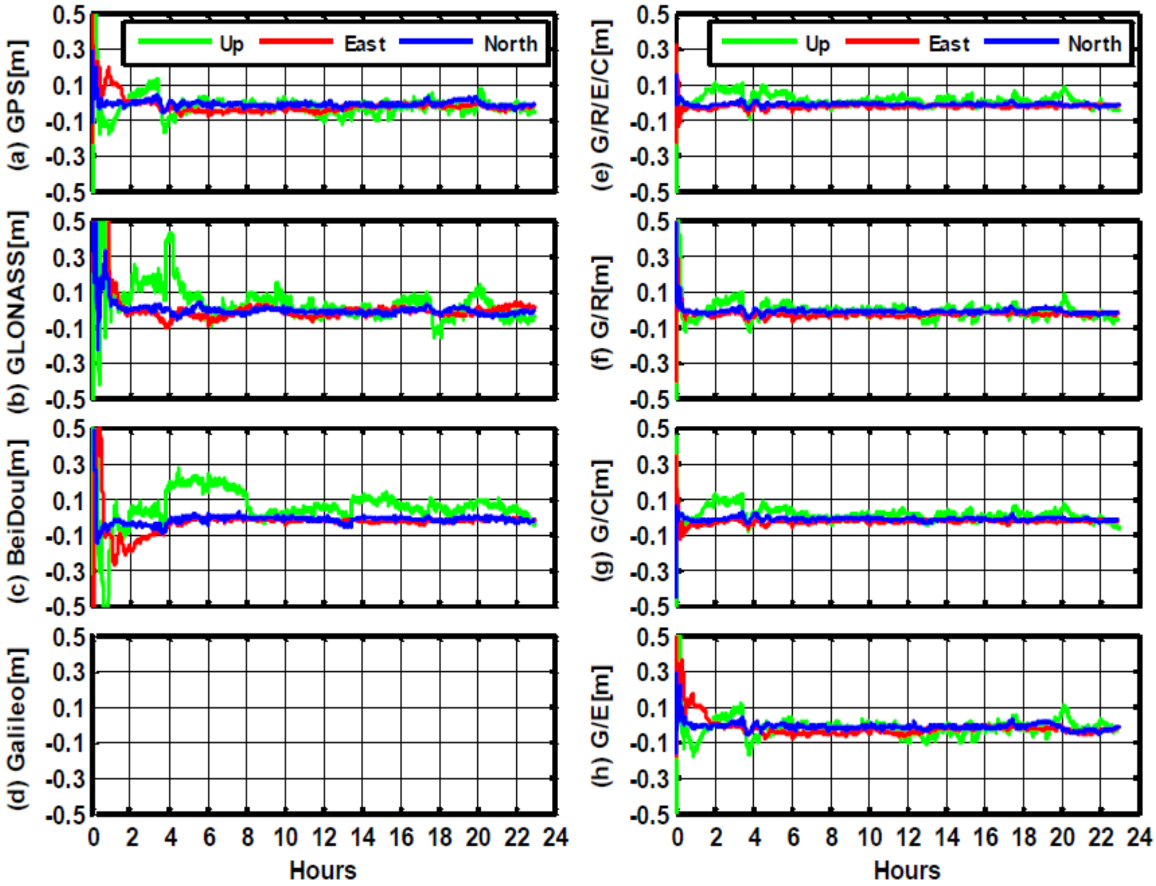

Figure 10. Kinematic PPP solutions of single-system, dual-system and four-system modes at station CUT0 (latitude: -32.00°, longitude: 115.89°, Australia), on September 1, 2013.

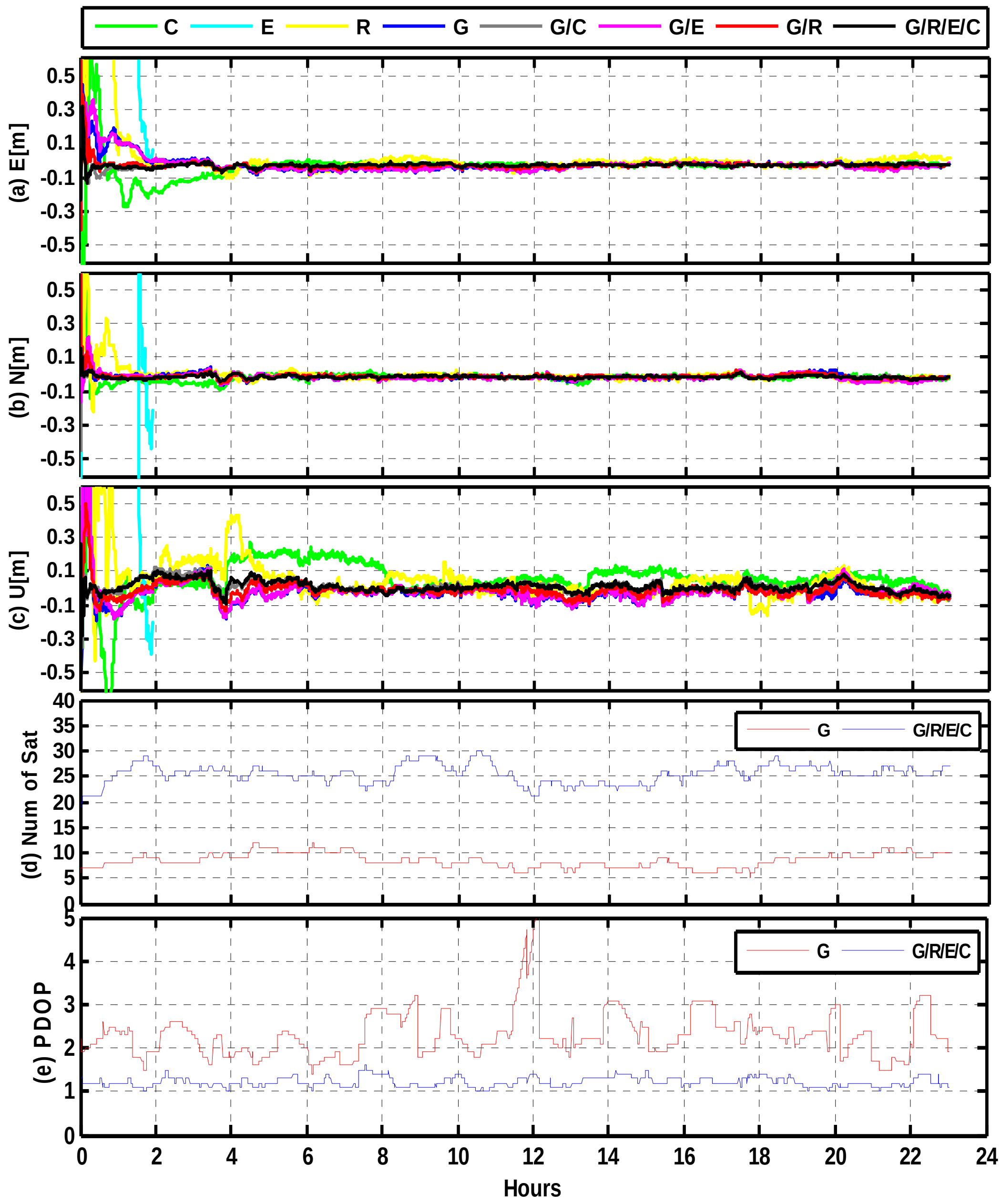

Figure 11． Comparisons of PPP results from different single-system and combined solutions in the east, north and up components, respectively at station CUT0. The corresponding satellite numbers and PDOP values are also shown.

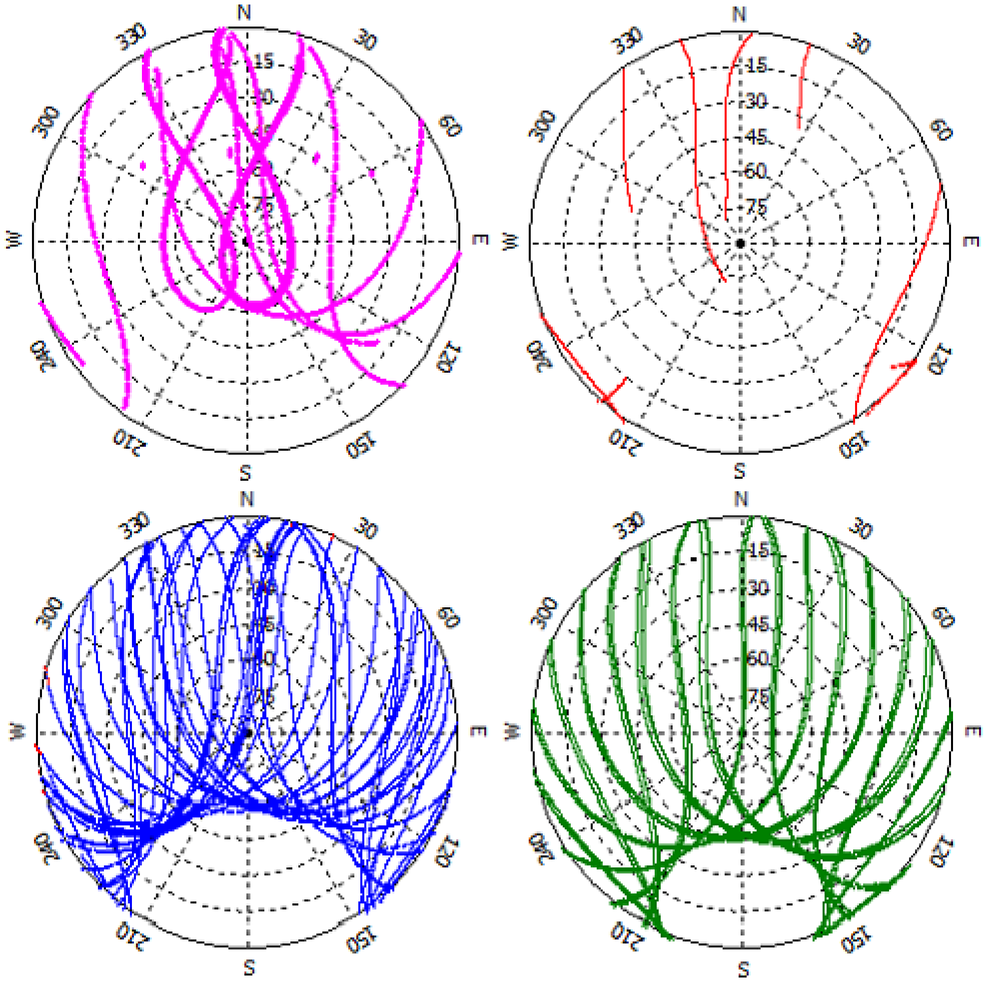

Figure 12. Sky plots (azimuth vs elevation) of the four GNSS (BeiDou in pink, Galileo in red, GPS in blue and GLONASS in green) for CUT0 on September 1, 2013

We analyzed the positioning accuracy of kinematic PPP solutions after convergence in single-, dual-, and four-system modes. The convergence periods are excluded to compute RMS values. The RMS values in east, north, and up are shown on Figure 13 for fourteen stations. For the single-system solutions, GPS has the best accuracy with horizontal accuracy better than 3.0 cm and vertical accuracy better than 1 dm. The GLONASS PPP accuracy is obviously worse than GPS, especially for GMSD and LMMF stations. The accuracy of BeiDou PPP is comparable to that of GPS PPP in horizontal components, but its vertical component is worse than GPS PPP especially for the station GMSD. It is worth to notice that some stations are out of the service area of BeiDou. Compared with single-system results, the positioning accuracy of multi-GNSS PPP is evidently improved. The horizontal accuracy of 1 cm can even be achieved for most of stations in the four-system PPP mode. The vertical accuracy is also generally better than 4 cm. The averaged RMS values of all the stations are also shown on Figure 14.

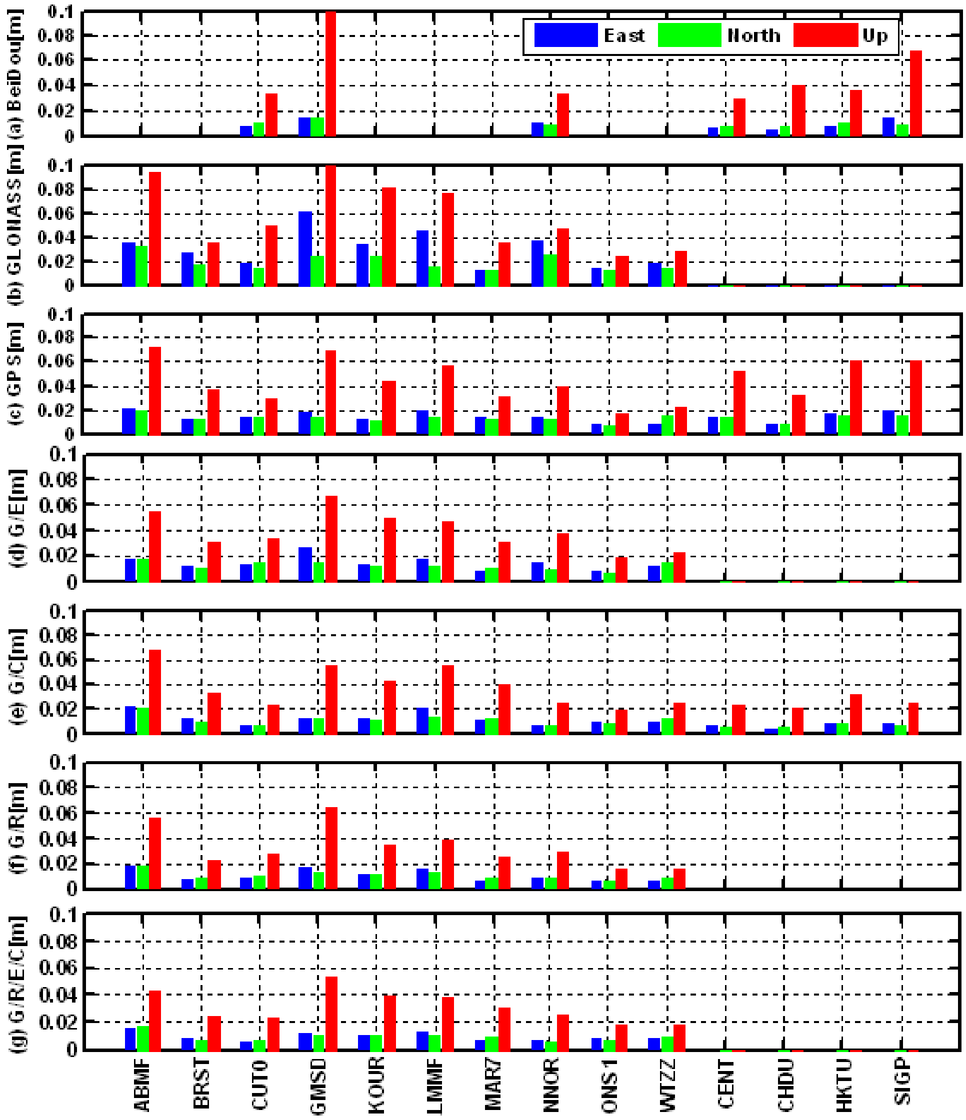

Figure 13．The accuracy of kinematic PPP solutions after convergence in single-, dual-, and four-system modes.

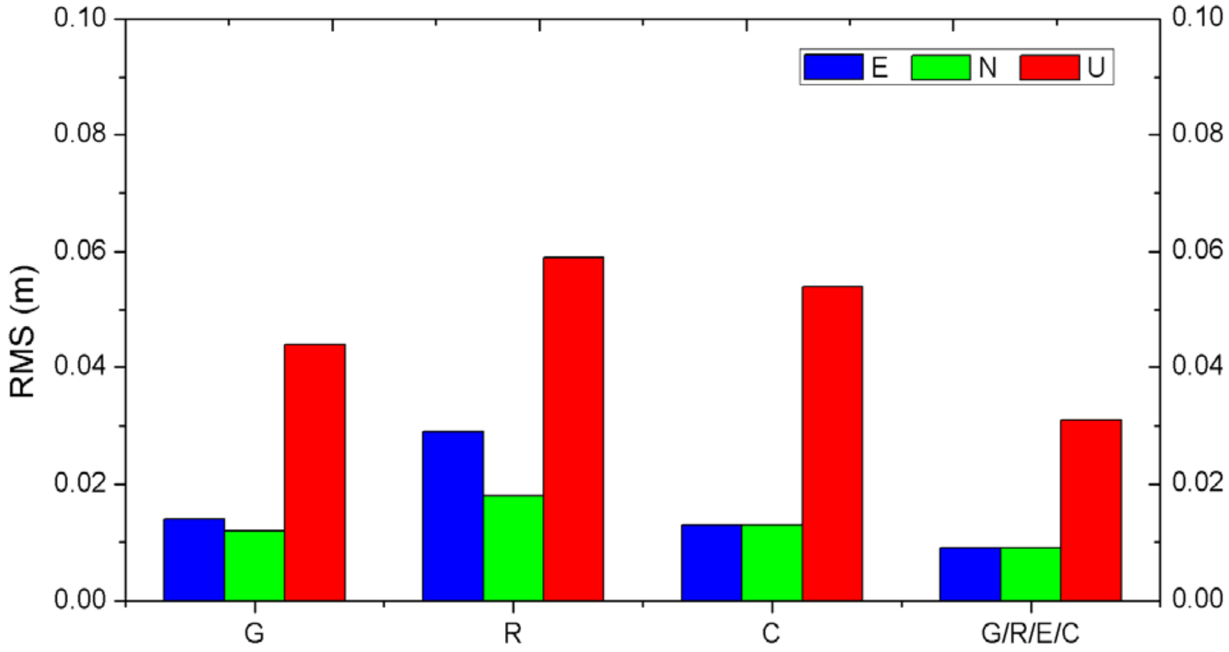

Figure 14. The averaged RMS values of all the stations for kinematic PPP solutions in north, east and up components.

We also analyzed the convergence time of all the PPP solutions for all the selected stations during the whole experimental period. Here a converged solution means that the horizontal accuracy is better than 0.1 m and the vertical accuracy is better than 0.2 m. The statistical results show that the convergence time is about 37, 58, and 59 minutes for GPS-only, GLONASS-only and BeiDou-only PPP, respectively. In contrast, the multi-GNSS solutions converge much faster than single-system solutions and about 18, 17 and 35 minutes are respectively required for GPS+GLONASS, GPS+BeiDou, and GPS+Galileo PPP. Furthermore, the GPS+GLONASS+BeiDou+Galileo four-system PPP convergence time is significantly reduced to only about 11 minutes. The important contribution of multi-GNSS to PPP convergence time will undoubtedly enhance its capability to time-critical applications.

As we know, the availability and reliability of GPS precise positioning decrease dramatically under some constrained conditions, for instance, deep open pit mines, urban canyons, and river valleys when not all available satellites are visible. In order to better understand as well as demonstrate the capabilities that a combining utilization of multi-GNSS systems brings to positioning, we analyzed the PPP performance in both single- and multi-system modes under different elevation cutoffs, ranging from 10° to 40°.

The PPP results, satellite numbers, and PDOP values for the four-system station CUT0 are shown as a typical example in Figure 15. For a 10° elevation cutoff, the results are very similar with abovementioned results (in which 7° is adopted as usual): 22~30 usable satellites, stable PDOP values below 1.5, 10 minutes convergence and horizontal accuracy of about 1cm in multi-GNSS PPP, while 5~10 usable satellites, PDOP variation from 2 to 6, about 40 minutes convergence and horizontal accuracy of about 2cm in GPS PPP. At 20° elevation cutoff, the averaged number of usable GPS satellites is reduced to 6 and the PDOP values are increased to be larger than 5 for several periods. Correspondingly, the GPS-only position series show larger fluctuations. In contrast, there are still more than 18 satellites in multi-PPP and the PDOP values are stable and around two. The position series is hardly affected and still very stable especially in the horizontal components. For a 30° elevation cutoff, only about five GPS satellites are visible and the PDOP values are even larger than ten for many periods. We can see that the positioning results are very unreliable and precise position estimates are frequently not available. Considering the multi-GNSS scenario, there are still more than 15 satellites visible and PDOP values are below three in general. Moreover, the horizontal position series are still very stable and accurate as those of 10° elevation cutoff, although the vertical position series present larger fluctuations along with the increase of elevation cutoff. When 40° elevation cutoff is adopted, just four satellites can be observed and PDOP values are larger than ten in most of time, the position series are fully disturbed and precise positioning service is not available for GPS. However, we can find that the multi-GNSS PPP position series are still not affected in horizontal components. It is reasonable that more than ten satellites can still be observed and PDOP values vary between three and six. It is worthwhile to note that the high IGSO and GEO satellites from BeiDou play a special role in this context as they have much longer tracking periods in the Asia-Pacific area. The PPP performance under different elevation cutoffs for some other stations is also shown in the Appendix II.

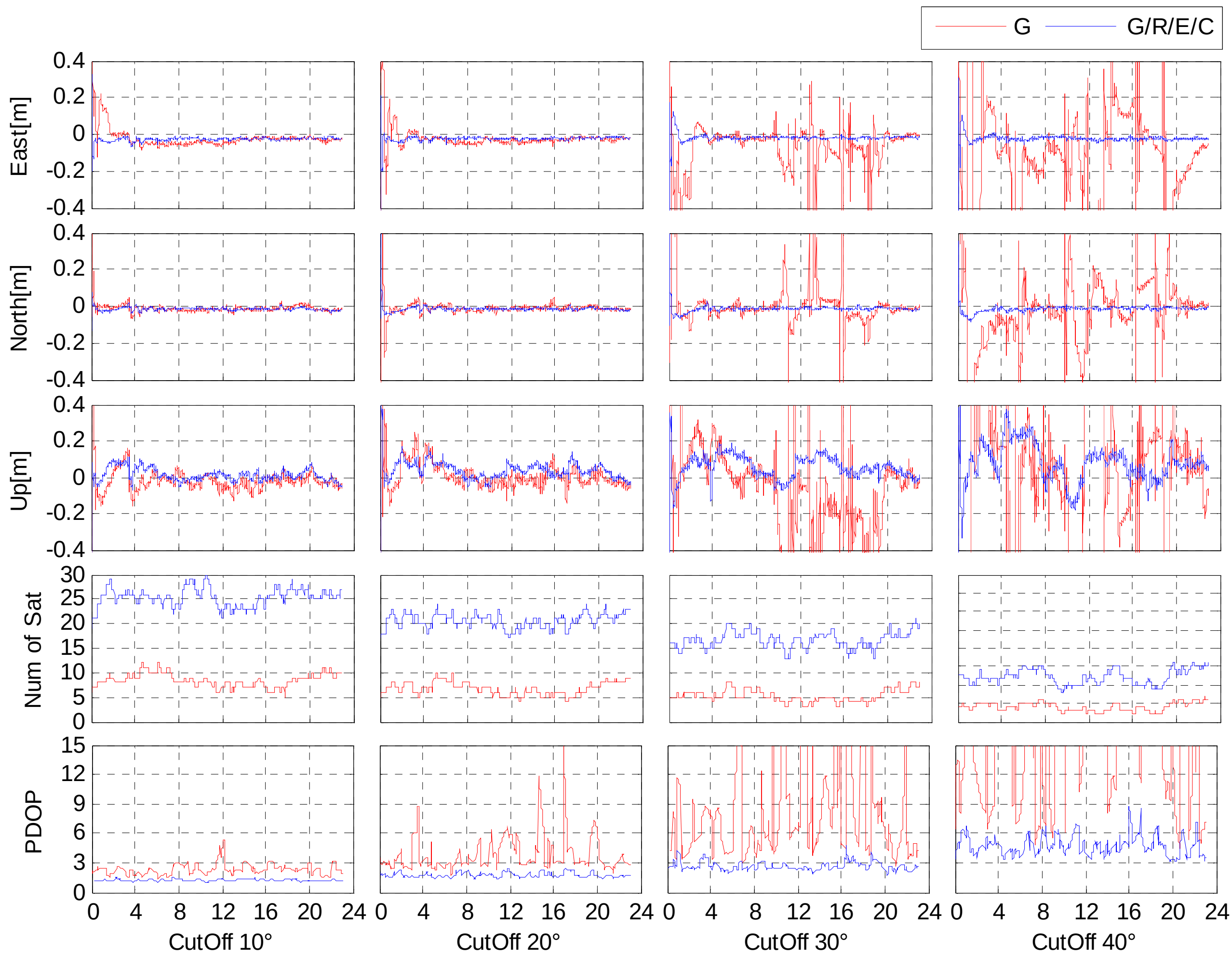

Figure 15. Comparisons of PPP results in single- and multi-system modes under different elevation cutoffs (from 10° to 40°) at station CUT0. The corresponding satellite numbers and PDOP values are also shown.

In order to further understand the significant contribution of multi-GNSS to reliability and availability especially in constrained environments, we define an empirical availability rate (EAR) as,

$$f_{availability} = \frac{N_{precise}}{N_{total}} \tag{22}$$

where $N_{precise}$ denotes the number of epochs with precise position estimates; N_{total} denotes the total number of epochs; $f_{availability}$ is the ratio of $N_{precise}$ and N_{total} to indicate the availability of precise position estimates.

The empirical availability rate $f_{availability}$ for the single- and multi-GNSS under different elevation cutoffs (from 10° to 40°) are computed to show how the availability-rates change when the elevation cutoff changes. The availability rates are derived from PPP solutions of all days for each station. Here precise position estimates means the position accuracy is better than 5 cm in both north and east components and the convergence periods are removed. The statistical results of some typical stations are shown in Table 9. As one would expect, the single-system availability rates all get smaller as the elevation cutoff gets larger. The GPS PPP can enable high precision positioning in more than 90% of the time when 10° elevation cutoff is used, while this decreases to several percent in case of 20° elevation cutoff. At 30° and 40° elevation cutoffs, the availability rates drop dramatically to only around 70% and 40% respectively. Table 9 also shows excellent results for all multi-GNSS cases. Precise position estimates are continuously available from multi-GNSS PPP even up to 40° elevation cutoff. At 10 and 20° elevation cutoff, the multi-GNSS enables high precision positioning for all the epochs (i.e. 100%). More than 99.5% can still be achieved with the multi-GNSS at higher elevation cutoffs even at 40° elevation cutoff.

From the previous analysis, it is clearly shown that the fusion of multiple GNSS can significantly increase the number of observed satellites, optimize the spatial geometry and improve convergence, accuracy, continuity and reliability of positioning. At the same time, much higher elevation cutoffs can be used with the multi-GNSS compared to single-system applications. This is important, since such capability will significantly increase the GNSS applicability in constrained environments.

Table 9. The empirical availability rates (in %) for the single- and multi-GNSS under different elevation cutoffs (from 10° to 40°)

Station	GPS（%）				G/R/E/C（%）			
	10°	20°	30°	40°	10°	20°	30°	40°
CENT	100.0	99.6	89.2	41.5	100.0	100.0	100.0	100.0
CHDU	99.7	98.3	84.7	46.0	100.0	100.0	100.0	100.0
SIGP	94.8	93.7	72.1	39.2	100.0	100.0	99.9	99.5
CUT0	96.8	95.0	89.3	57.6	100.0	100.0	100.0	100.0
GMSD	98.1	97.6	79.5	30.2	100.0	100.0	100.0	99.8
NNOR	99.2	93.8	78.6	37.8	100.0	100.0	100.0	100.0
ONS1	96.1	93.3	62.5	30.6	100.0	100.0	99.9	99.6

5 Conclusions

With the rapid development of multi-GNSS, 74 satellites are available in August 2014, transmitting more data for high precision PNT applications than during past years with 32 GPS satellites only. Once all four systems are fully deployed, more than 100 satellites will be available. Recently, GFZ put on much effort on developing its real-time service for multi-GNSS applications. In this contribution, we present a GPS+GLONASS+BeiDou+Galileo four-system model for real-time PPP as well as POD and PCE. Meanwhile, an efficient multi-GNSS real-time precise positioning service system is designed and demonstrated. A rigorous multi-GNSS analysis is performed to achieve the best possible consistency by processing the observations from different GNSS together in one common parameter estimation procedure.

The MGEX+BETN+IGS networks including stations all over the world provide a great opportunity for our experimental study. The overlap (two adjacent three-day solutions) RMS values of estimated

Galileo orbit are about 2.1, 3.7 and 7.8 cm respectively in radial, cross and along components, which is worse than both GPS and GLONASS because of a limited number of tracking stations. The overlap RMS values of BeiDou IGSO satellites are about 2.5, 3.3, and 4.4 cm in radial, cross and along components, respectively, which is comparable to the Galileo results. The RMS values of MEO are 3.4, 4.3 and 11.3 cm in the radial, cross, and along directions, respectively. The GEO satellites have similar performance with IGSO and MEO satellites in the radial and cross directions, however, the accuracy of along component is significantly decreased to nearly 1 m due to the rather weak geometry. This situation is expected to improve if some spaceborne BeiDou observations (e.g. from LEO satellites) are available.

The statistical results of the 6 h predicted orbits show that the along-track component is still the worst of the three directions, especially for GEO satellites. However, the radial and cross RMS values are smaller than 10 cm for BeiDou and Galileo, and smaller than 5 cm for both GLONASS and GPS satellites, respectively. The predicted orbit accuracy is generally several centimeters worse than estimated orbit. The RMS values of clock differences between the real-time and batch-processed solutions for GPS satellites are about 0.10 ns, while the RMS values of BeiDou, Galileo and GLONASS are 0.13, 0.13 and 0.14 ns, respectively. The results confirm that both satellite orbits and clocks can achieve an accuracy at cm level in real-time. In addition, the errors of orbits and clocks can be compensated by each other when they are used together at user end.

Based on the predicted orbit and real-time estimated clocks, precise point positioning can be performed to validate the capability of real-time precise positioning service. The multi-GNSS PPP presents faster convergence and higher accuracy in all the three components than single-system PPP, thanks to the increasing of satellite numbers and the improvement of the PDOP values. Generally speaking, about five to ten satellites can be used for GPS-only solution and the variation PDOP is from 2 to 6. In contrast, the observed satellite numbers for multi-GNSS solution with four systems are between 22 and 30 and the PDOP values are below 1.5 and very stable. The addition of BeiDou, Galileo and GLONASS systems to the standard GPS-only processing, almost cut 70% of the convergence time, while the positioning accuracy is improved by about 25%. Meanwhile, the position series of multi-PPP are much more stable than GPS-only solutions, with much fewer fluctuations. Some spikes, visible in GPS-only solutions, can be easily solved when multi-GNSS observations are processed simultaneous.

We also analyze the real-time positioning capabilities of the combined systems under different elevation cutoffs, ranging from 10° to 40°. The satellite number gets smaller and PDOP gets larger as the elevation cutoff gets larger. The availability and reliability of GPS-only precise positioning decrease dramatically as the elevation cutoff increases. Importantly though, the PDOP of the multi-GNSS remains small for large elevation cutoffs. The positioning accuracy of multi-GNSS PPP hardly decreases and few centimeter accuracy is still achievable in horizontal components even with a 40° elevation cutoff. At 30° and 40° elevation cutoffs, the availability rates of GPS-only solution drop dramatically to only around 70% and 40% respectively. However, multi-GNSS PPP shows excellent results. In particular, precise position estimates are continuously available even up to 40° elevation cutoff. At 10° and 20° elevation cutoffs, the multi-GNSS enables high precision positioning for all the epochs (i.e. 100%). More than 99.5% can still be achieved with the multi-GNSS at higher elevation cutoffs even at 40° elevation cutoff.

From the previous analysis, it is clearly shown that the fusion of multiple GNSS significantly increases the number of observed satellites, optimizes the spatial observation geometry at a site and improves convergence, accuracy, continuity and reliability of positioning. Especially, the high elevation cutoff capability of multi-GNSS will significantly increase its applicability in constrained environments, such as e.g. in urban canyons, open pits or when serious low-elevation multipath is present. It is worthwhile to note that the constellations of BeiDou and Galileo are still uncompleted, the multi-GNSS tracking stations are not evenly distributed, and not all the stations can track four systems at the moment. Therefore, the performance of the multi-GNSS processing will be further improved in the next years along with the launch of more satellites and the setup of more multi-GNSS stations.

Acknowledgements. We are very grateful to IGS, MGEX, WHU and HuBei CORS for providing multi-GNSS data.

Appendix I

Figure A1 shows the kinematic PPP results for another four-system station GMSD, which is located in Japan. The PPP solutions related to GPS, GLONASS and BeiDou have similar performance compared to the results of CUT0 station. As shown in Figure A1d, Galileo-only PPP is achievable for few hours even with four satellites. The accuracy of several centimeters can be obtained for about 2-3 hours, although currently it is not possible to use Galileo as a stand-alone system for continuous positioning. Meanwhile, as shown in Figure A1h, Galileo also provides a contribution to some extent for PPP solutions when used together with e.g. GPS. The sky plots (azimuth vs elevation) of four systems for GMSD are shown in Figure A2.

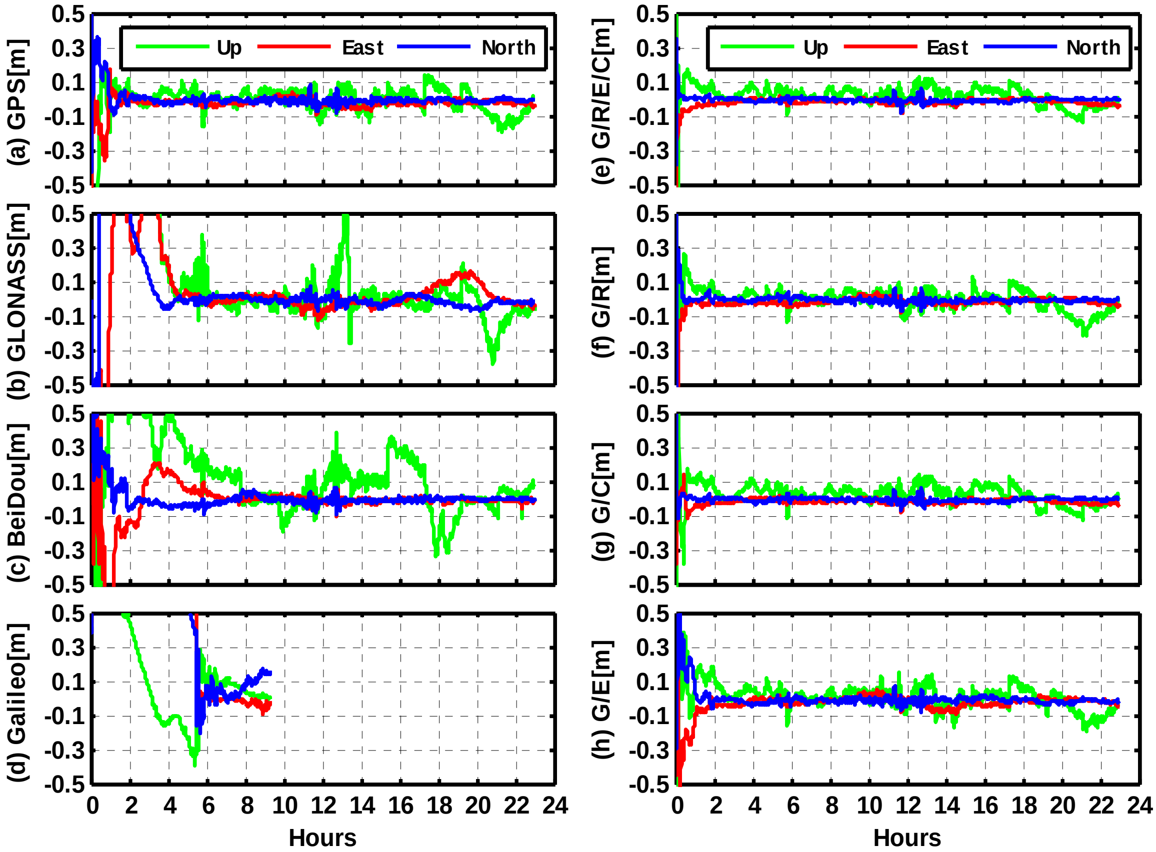

Figure A1. Kinematic PPP solutions of single-system, dual-system and four-system modes at station GMSD (latitude: 30.55°, longitude: 131.01°, Japan, Asia), on September 1, 2013.

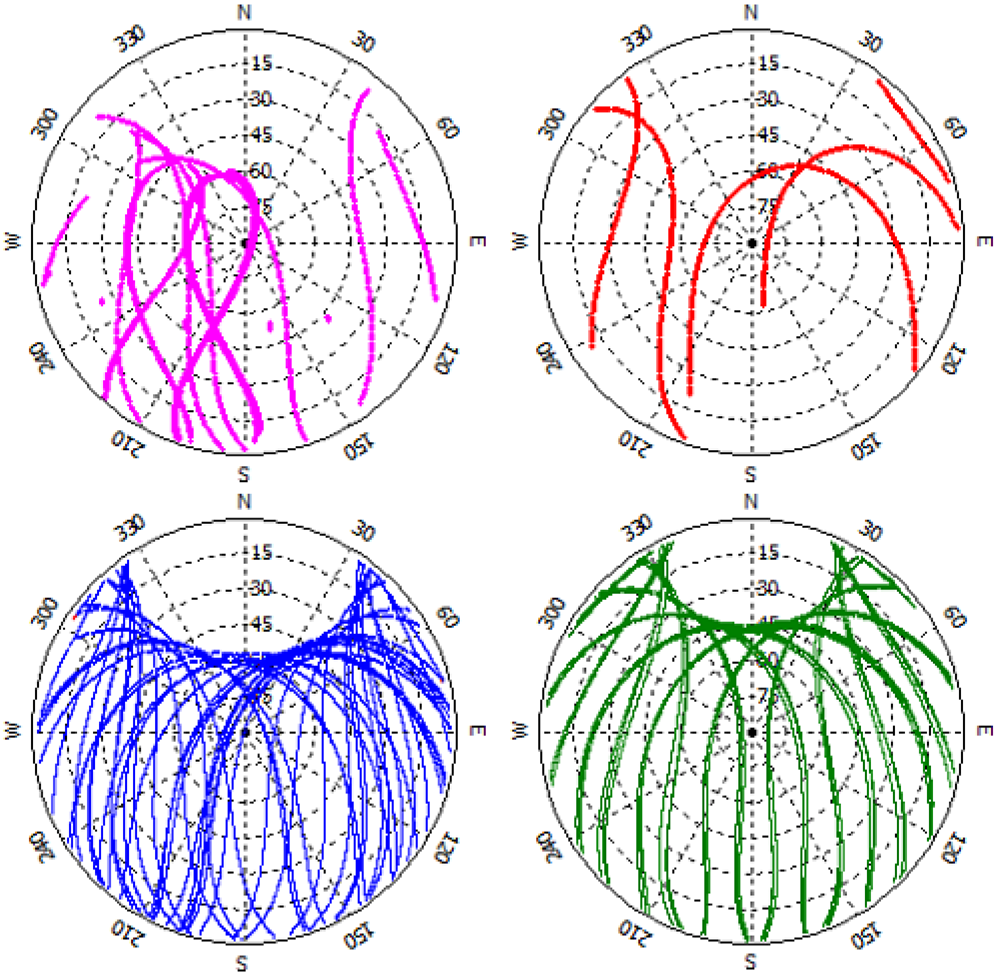

Figure A2. Sky plots (azimuth vs elevation) of four GNSS (BeiDou in pink, Galileo in red, GPS in blue and GLONASS in green) at GMSD on September 1, 2013

Figure A3 shows the kinematic PPP results for another four-system station LMMF located in Latin America with latitude of -14.59° and longitude of -60.99°. At this location, both Beidou and Galileo cannot provide continuous positioning as a stand-alone system and only few hours of Beidou-only and Galileo-only PPP are obtainable, as shown in Figure A3c and A3d. However, the PPP solutions can converges faster and achieve more accurate position series when Beidou or Galileo are combined together with GPS, as demonstrated in Figure A3g and A3h.

The PPP accuracy with different observational lengths (e.g. 0.25, 0.5, 1, and 2 h) is compared in

Figure A4. The accuracy of single-system PPP is improved along with the observational lengths. If data of 2 hours or longer are involved in the processing, position accuracy of few centimeters can be achieved. For multi-GNSS PPP, the accuracy of few centimeters is already available in all the three components with observational length of 0.25 h and then stays on cm-level.

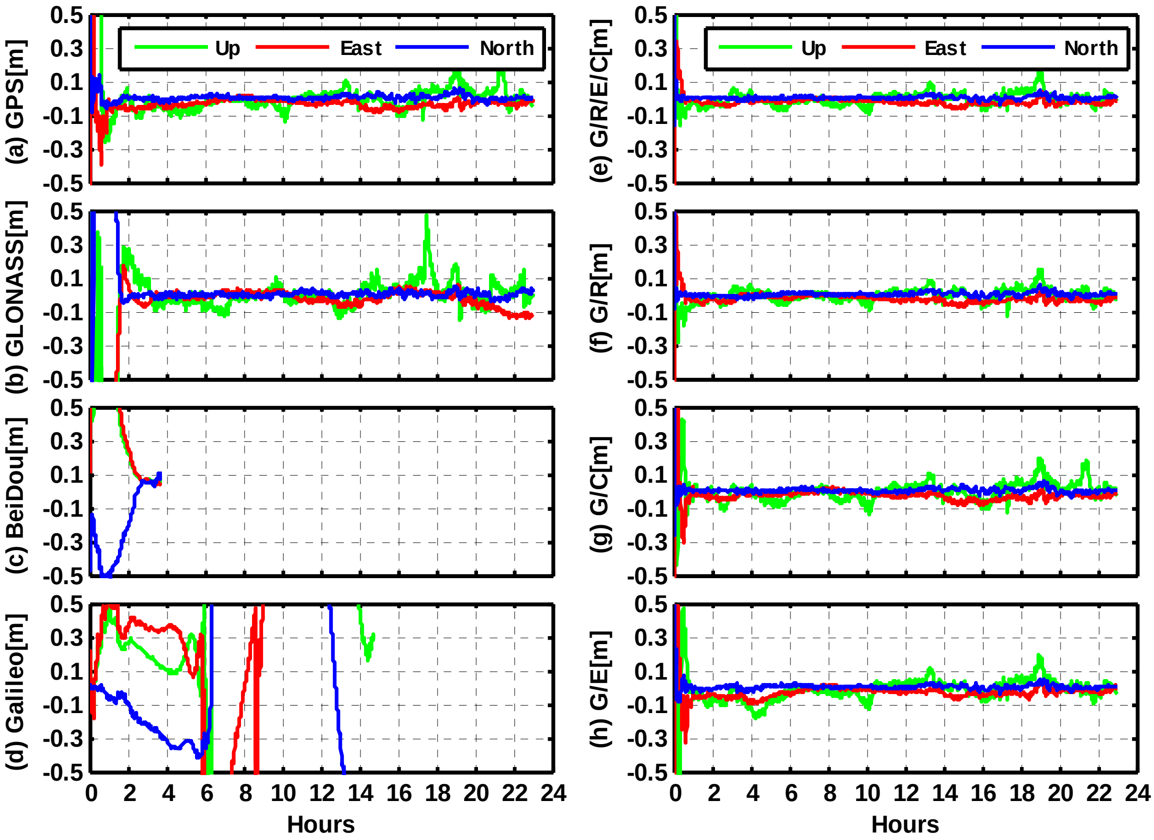

Figure A3. Kinematic PPP solutions of single-system, dual-system and four-system modes at station LMMF (latitude: 14.59°, longitude: -60.99°, Martinique, Latin America), on September 1, 2013.

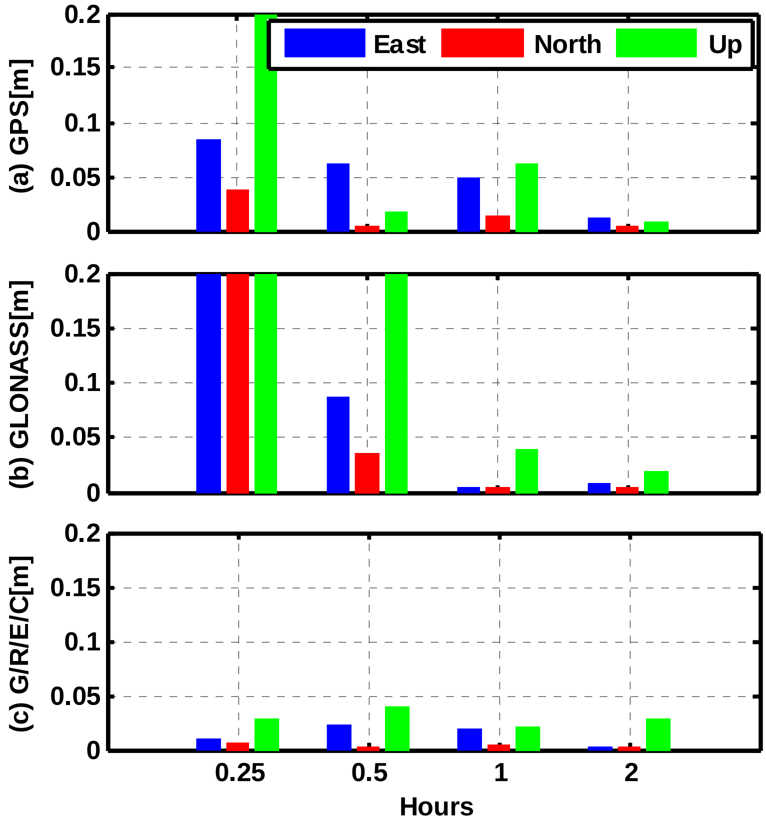

Figure A4. Position errors of kinematic PPP solutions at station LMMF with different observational lengths of 0.25, 0.5, 1, and 2 hours in single-system and multi-GNSS modes.

Appendix II

Figure A5 shows the PPP results, satellite numbers, and PDOP values under different elevation cutoffs for another four-system station GMSD. It has similar performance as the station CUT0: PDOP gets larger as the elevation cutoff gets larger. The availability and reliability of GPS precise positioning decrease dramatically as the elevation cutoff increases. Importantly though, the PDOP of the multi-GNSS remains small for large elevation cutoffs. Furthermore, the positioning accuracy of multi-PPP is nearly not decreased and few centimeters are still achievable in horizontal components even with 40° elevation cutoff. The vertical accuracy decreases gradually as the elevation cutoff increases.

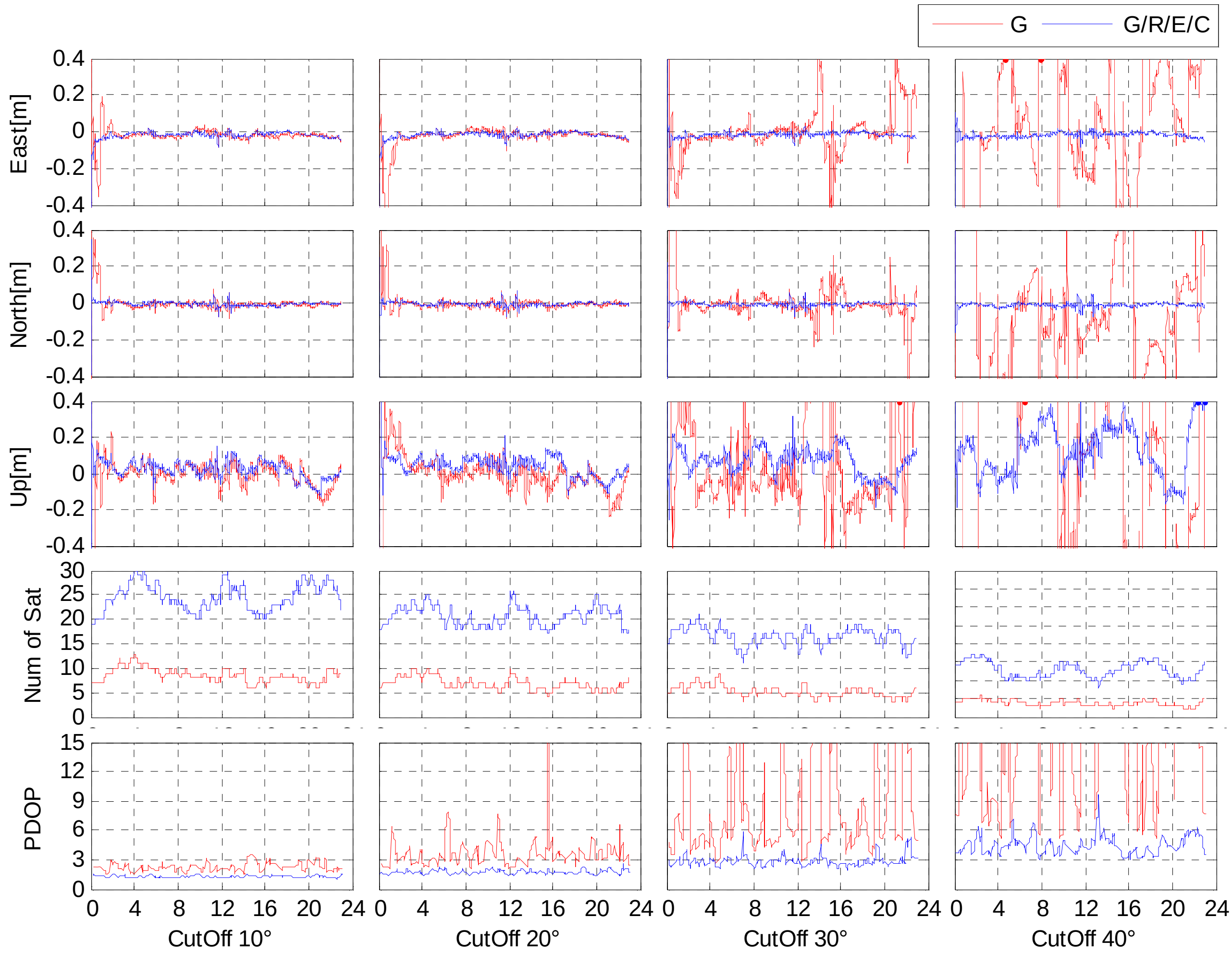

Figure A5. Comparisons of PPP results in single- and multi-system modes under different elevation cutoffs (from 10° to 40°) at station GMSD. The corresponding satellite numbers and PDOP values are also shown.

We also present the PPP results under different elevation cutoffs for the dual-system station CENT in Figure A6. With elevation cutoff of 20°, there is a obvious spike in the north components of GPS PPP due to the reduction of observable satellites to only four, while GPS+BeiDou PPP does not present any decrease in accuracy. When the elevation cutoff is increased to 30° or 40°, reliable GPS PPP is not achievable. The position series of combined PPP are only a little nosier for 30° elevation cutoff. They are much nosier at 40°, but the accuracy of centimeter lever can still be obtained in horizontal components. Compared with the Figures A5 , although the dual-system PPP solutions are not as stable and robust as the four-system PPP, the convergence time, PNT accuracy and reliability benefits from adding BeiDou.

Figure A6. Comparisons of PPP results in single- and dual-system modes under different elevation cutoffs (from 10° to 40°) at station CENT. The corresponding satellite numbers and PDOP values are also shown.

References

Al-Shaery A, Zhang S, Rizos C (2013) An enhanced calibration method of GLONASS inter-channel bias for GNSS RTK. GPS Solut 17(2):165–173. doi:10.1007/s10291-012-0269-5

Altamimi Z, Collilieux X, Métivier L (2011) ITRF2008: an improved solution of the international terrestrial reference frame. J Geod 85(8):457-473, DOI 10.1007/s00190-011-0444-4

Cai C, Gao Y (2013) Modeling and assessment of combined GPS/GLONASS precise point positioning. GPS Solut 17(2):223–236

Caissy M, Agrotis L, Weber G, Hernandez-Pajares M, Hugentobler U (2012), Coming Soon: The International GNSS Real-Time Service, GPS World, Jun 2012, Vol. 23 Issue 6, p52-58.

Chen X, Landau H, Zhang F, Nitschke M, Glocker M, Kipka A, Weinbach U, Salazar D (2013) Towards a Precise Multi-GNSS Positioning System Enhanced for the Asia-Pacific Region. LECTURE NOTES IN ELECTRICAL ENGINEERING, 245, 277-290, China Satellite Navigation Conference (CSNC)

Dach R, Schaer S, Hugentobler U (2006) Combined multi-system GNSS analysis for time and frequency transfer. Proc. Eur. Freq. Time Forum, 2006, pp. 530 – 537

Dow JM, Neilan RE, Rizos C (2009) The International GNSS Service in a changing landscape of Global Navigation Satellite Systems, J Geod, 83:191-198, DOI: 10.1007/s00190-008-0300-3.

Ge M, Gendt G, Rothacher M, Shi C, Liu J (2008) Resolution of GPS carrier-phase ambiguities in precise point positioning (PPP) with daily observations, J Geod. 82(7):389-399. doi:10.1007/s00190-007-0187-4.

Ge M, Zhang HP, Jia XL, Song SL, Wickert J (2012) What Is Achievable with the Current COMPASS Constellation? GPS World November, p29-34.

Hauschild A, Montenbruck O, Sleewaegen JM, Huisman L, Teunissen PJG (2012) Characterization of Compass M-1 signals. GPS Solut. 16, 117-126.

He H, Li J, Yang Y, Xu J, Guo H, Wang A (2013a) Performance assessment of single- and dual-frequency BeiDou/GPS single-epoch kinematic positioning. GPS Solut. 18(3):393-403

He L, Ge M, Wang J, Wickert J, Schuh H (2013b) Experimental study on the precise orbit determination of the BeiDou navigation satellite system. Sensors 13(3):2911–2928. doi:10.3390/s130302911

Kouba, J. (2009) A Guide to Using International GNSS Service (IGS) Products, http://igscb.jpl.nasa.gov/igscb/resource/pubs/UsingIGSProductsVer21.pdf.

Li X, Zhang X, Ge M (2011) Regional reference network augmented precise point positioning for instantaneous ambiguity resolution. J Geod. 85, 151-158.

Li X, Ge M, Zhang H, Nischan T, Wickert J (2013a) The GFZ real-time GNSS precise positioning service system and its adaption for COMPASS. Adv Space Res 51(6):1008–1018

Li X, Ge M, Zhang H, Wickert J (2013b) A method for improving uncalibrated phase delay estimation and ambiguity-fixing in real-time precise point positioning. J Geod. 87(5):405-416. doi:10.1007/s00190-013-0611-x.

Li X, Ge M, Zhang X, Zhang Y, Guo B, Wang R, Klotz J, Wickert J (2013c) Real-time high-rate co-seismic displacement from ambiguity-fixed precise point positioning: Application to earthquake early warning. Geophys Res Lett 40(2):295–300. doi:10.1002/grl.50138

Li X, Dick G, Ge M, Heise S, Wickert J, Bender M (2014) Real-time GPS sensing of atmospheric water vapor: Precise point positioning with orbit, clock, and phase delay corrections. Geophys Res Lett 41(10):3615-3621. doi:10.1002/2013GL058721

Li X, Zhang X, Ren X, Fritsche M, Wickert J, Schuh H (2015) Precise positioning with current multi-constellation Global Navigation Satellite Systems: GPS, GLONASS, Galileo and BeiDou. Sci Rep., 5, 8328.

Liu J, Ge M (2003), PANDA software and its preliminary result of positioning and orbit determination. Wuhan University Journal of Natural Sciences 8, 603-609.

McCarthy D, Petit G (2003) IERS Conventions, IERS technical note No. 32; Publisher of the Federal Agency for Cartography and Geodesy: Frankfurt am Main, Germany.

Montenbruck O, Hauschild A, Steigenberger P, Hugentobler U, Teunissen P, Nakamura S (2012), Initial assessment of the COMPASS/BeiDou-2 regional navigation satellite system. GPS Solut. 17(2):211-222, DOI 10.1007/s10291-012-0272-x.

Montenbruck O, Steigenberger P, Khachikyan R, Weber G, Langley RB, Mervart L, Hugentobler U (2014) IGS-MGEX: preparing the ground for multi-constellation GNSS science. Inside GNSS, 9 (1), pp. 42 – 49

Odijk D, Teunissen PJG (2013) Characterization of between-receiver GPS-Galileo inter-system biases and their effect on mixed ambiguity resolution. GPS Solut. 17(4):521-533. doi:10.1007/s10291-012-0298-0

Schaer S, Beutler G, Rothacher M, Brockmann E, Wiger A, Wild U (1999) The impact of the atmosphere and other systematic errors on permanent GPS networks. Pres. IAG Symp on Positioning, Birmingham, UK, 19-24 July, 406.

Schaffrin B, Bock Y (1988), A unified scheme for processing GPS dual-band phase observations. Bull. Geod. 62 pp. 142-160.

Shi C, Zhao Q, Li M, Tang W, Hu Z, Lou Y, Zhang H, Niu X, Liu J (2012), Precise orbit determination of BeiDou Satellites with precise positioning. Science China Earth Sciences 55, 1079-1086.

Steigenberger P, Hugentobler U, Montenbruck O, Hauschild A (2011), Precise orbit determination of GIOVE-B based on the CONGO network. J Geod. 85, 357-365.

Teunissen PJG, Odolinski R, Odijk D (2014) Instantaneous BeiDou+GPS RTK positioning with high cut-off elevation angles. J Geod. 88(4):335-350 doi:10.1007/s00190-013-0686-4

Yang YX, Li JL, Xu JY, Tang J, Guo HR, He HB (2011), Contribution of the Compass satellite nagivation system to global PNT users, Chinese Science Bulletin 56(26), 2813-2819, doi:10.1007/s11434-001-4627-4.

Zhang X, Li X, Guo F (2011). Satellite Clock Estimation at 1 Hz for Realtime Kinematic PPP applications. GPS Solut. 15(4), 315-324, doi: 10.1007/s10291-010-0191-7.

Zhao Q, Guo J, Li M, Qu L, Hu Z, Shi C, Liu J (2013). Initial results of precise orbit and clock determination for COMPASS navigation satellite system. J Geod. 2013, 5, 475–486.

Zumberge JF, Heflin MB, Jefferson DC, Watkins MM, Webb FH (1997). Precise point positioning for the efficient and robust analysis of GPS data from large networks, J. Geophys. Res. 102(B3):5005-5017. doi:10.1029/96JB03860.